International Journal of Nanomedicine

Dovepress
open access to scientific and medical research

Open Access Full Text Article

ORIGINAL RESEARCH

Nanostructured Ag^+-substituted fluorhydroxyapatite-TiO_2 coatings for enhanced bactericidal effects and osteoinductivity of Ti for biomedical applications

This article was published in the following Dove Press journal:
International Journal of Nanomedicine

Yong Huang[1,*]
Guiqin Song[1,*]
Xiaotong Chang[1]
Zhenhui Wang[2]
Xuejiao Zhang[1]
Shuguang Han[3]
Zhuobin Su[4]
Hejie Yang[5]
Dongdong Yang[6]
Xiaojun Zhang[7]

[1]College of Lab Medicine, Hebei North University, Zhangjiakou, China; [2]Department of Nuclear Medicine, People's Liberation Army No 251 Hospital, Zhangjiakou, China; [3]Institute of Life Science and Technology, University of Electronic Science and Technology of China, Chengdu, China; [4]The First Affiliated Hospital, Hebei North University, Zhangjiakou, China; [5]State Key Laboratory for Mechanical Behavior of Materials, Xi'an Jiaotong University, Xi'an, China; [6]School of Physics and Optoelectronic Engineering, Ludong University, Yantai, China; [7]Department of Physics, Fourth Military Medical University, Xi'an, China

*These authors contributed equally to this work

Correspondence: Xiaojun Zhang
Department of Physics, Fourth Military Medical University, No. 169, Changle West Road, Xi'an 710032, China
Tel/fax +86 29 8477 4834
Email zy04310@fmmu.edu.cn

Background: Poor mechanical properties, undesirable fast dissolution rate, and lack of antibacterial activity limit the application of hydroxyapatite (HA) as an implant coating material. To overcome these limitations, a hybrid coating of Ag^+-substituted fluorhydroxyapatite and titania nanotube (TNT) was prepared.

Methods: The incorporation of silver into the HA-TiO_2 hybrid coating improves its antimicrobial properties. The addition of F as a second binary element increases the structural stability of the coating. The TNT/F-and-Ag-substituted HA (FAgHA) bilayer coating on the Ti substrate was confirmed by X-ray diffraction, scanning electron microscope, energy-dispersive X-ray spectroscopy (EDS), and X-ray photoelectron spectroscopy (XPS).

Results: The results indicate that the FAgHA/TNT nanocomposite coating has a dense and uniform morphology with a nano-rod-like structure. The solubility measurement result shows that the substitution of F^- ions into the AgHA structure has a positive effect on the dissolution resistance of HA. The adhesion strength of FAgHA/TNT has significantly increased because of the interlocking of the roughened surface with nano-rod-like particles that entered into the voids of the TiO_2 nanotubes. Compared with that of the bare Ti, the corrosion current density of FAgHA/TNT-coated Ti substrate decreased from 3.71 to 0.18 μA, and its corrosion resistance increased by almost two orders of magnitude. Moreover, despite pure HA, the FAgHA killed all viable *Staphylococcus aureus* after 24 hours of incubation. Although the fabricated FAgHA/TNT coating is hydrophobic, it induced deposition of the typical spherical apatite when immersed in a simulated body fluid (SBF); the osteoblasts spread very well on the surface of the coating. In addition, in vitro cell culture tests demonstrated cell viability and alkaline phosphatase (ALP) similar to pure HA, which indicated good cytocompatibility. Interestingly, compared with bare Ti, FAgHA/TNT-coated Ti surface was innocent for cell vitality and even more beneficial for cell osteogenesis in vitro.

Conclusion: Enhancing the osseointegration and preventing infection in implants, the FAgHA/TNT-coated Ti makes implants more successful.

Keywords: titania nanotube, silver, fluorhydroxyapatite, bactericidal effects, osteoinductivity

Introduction

Owing to their excellent biological and mechanical properties, commercially pure titanium (CP-Ti) and Ti alloys (Ti6Al4V) have widely been in use as endosseous implants in clinics.[1,2] However, Ti lacks antimicrobial properties and sufficient osteogenic activity, which leads to a delayed osseointegration and complicated bacterial infections – which

submit your manuscript | www.dovepress.com
Dovepress
http://dx.doi.org/10.2147/IJN.S162558

consequently may make implants fail, particularly in patients with complex pathologies.[3,4] This negative effect of metallic implants has been reduced with the application of coatings of bioactive calcium phosphates (Ca-P) such as hydroxyapatite (HA) with the chemical formula of $Ca_{10}(PO_4)_6(OH)_2$.[5] The HA coatings on metal implants can provide a suitable substrate for the growth of bone; such coatings not only allow for tight chemical bonds at the bone/implant interface but also can act as a barrier between body fluids and the metallic implant.[6]

The in vivo success of a coated implant depends on several factors; the surface topography, that is, surface roughness and porosity, can strongly influence biological processes like protein adsorption, cell adhesion, and cell spreading;[7] moreover, the proliferation of osteoblasts, vascular ingrowth, and the subsequent bone formation can be further enhanced by an interconnected porous coating layer;[8] the interconnected porousness of the coating may make the implant suffer from bacterial activity in the early stages after the implantation, which may require additional medical operations for retrieving the implant.[9] In addition, HA is faced with an intrinsically high dissolution rate in a biological environment and poor corrosion resistance in acid solutions,[10] which is detrimental for long-term implant stability. Furthermore, the strength of the bonding between the coating and the metallic substrate can also affect the in vivo success of a coated implant;[5] that is, mechanical properties of the coated implant can be improved by the chemical bonds and/or inter-diffusion of elemental species of the HA and metals at the HA–metal interface.[4]

To overcome these problems, minerals with antimicrobial properties, the ability to induce new bone formation, and the effect of lowering the fracture risk in osteoporosis can be substituted into the HA.[9] These substitutions may bring about changes in the crystal structure and material properties like phase stability and reactivity. The substitution of Zn^{2+} and Sr^{2+} for Ca^{2+}, SiO_4^{4-}, and CO_3^{2-} for PO_4^{3-}, and F^- for OH^- stimulates the adhesion of bone cells to the implant and enhances the coating stability.[11] Being known for their strong inhibition of bacterial activities,[9] Ag ions, even in low amounts, can improve antibacterial properties of the HA.[12] However, the toxicity of high amounts of Ag beyond a critical value may lead to cell death.[9] In view of the high flexibility of the apatite structure, a great variety of cationic and anionic species can be incorporated into the HA structure – an effective method to modify the properties of HA.[9] Ag ions of radius 1.28 Å are substituted for Ca ions of radius 0.99 Å, which increases the lattice parameters.[9] It is worth noting that the incorporation of F^- into the HA structure reduces its unit cell volume and dissolution rate and increases its hardness[13] – therefore, partial substitution of F^- for OH^- ions, which results in $Ca_{10}(PO_4)_6(OH)_{2-x}F_x$, is one way for enhancing the structural stability of a HA coating, and for decreasing its in vivo dissolution rate.[15] In vitro studies indicate that the F^- for $-OH^-$ substitution induces greater cell proliferation and reduces bacterial proliferation.[14] Therefore, the mechanical and biological behavior of apatite coatings in metallic implants can be improved for biomedical applications.[17] A strategy that is worth pursuing is to fabricate a novel F-and-Ag-substituted HA (FAgHA) coating of implants that can have a good chemical stability with enhanced antibacterial properties.

Electrodeposition (ED) is one of the most promising approaches for fabricating HA coatings on Ti.[6] Several studies have reported the electrodeposited co-substitution of two distinct ions such as Sr/Mg, Cu/Zn, Na/Si, and F/Sr, into HA coating.[18] However, the major challenge of this method is the weak bond strength between the doped HA coating and the substrate.[19] The use of TiO_2 in the coating structure can improve the adhesion and corrosion behavior of the contacting layer.[20–22] In some cases, an intermediate layer of TiO_2 is formed by anodization between the HA deposit and the substrate. The porosity of the layer can enhance the HA adhesion and create suitable cell anchorage circumstances.[20,21]

We have already reported that AgHA/TiO_2 nanocomposite coatings can promisingly deactivate bacteria to lose their replication ability, which leads to cell death and significant bactericidal activity against gram-negative bacteria.[23–26] In addition, we previously employed ED to synthesize fluorhydroxyapatite (FHA)/ZrO_2 nanocoatings on Ti;[27] this ED-fabricated nanocomposite coating exhibited superior mechanical and chemical stability and stronger corrosion resistance than the pure HA film in physiological environments.[27] To the best of our knowledge, there have so far been no reported use of ED for the co-substitution of F and Ag into the HA coating on TiO_2 nanotube arrays. The present research was aimed at fabricating an FAgHA-TiO_2 (FAgHA/TNT) nanocomposite bilayer coating that can simultaneously offer the advantages of both TiO_2 and FAgHA. We aim 1) to synthesize the coating without the decomposition of the HA and without the formation of metallic silver and 2) to develop a fabrication method for the FAgHA coating that has a nanostructure with the use of the ED technique at a low processing temperature to combine cytocompatibility with antibacterial properties. The characterization of material properties, antibacterial performance, and cell adhesion behavior of the coating provides us with the data on its possible use in biomedical applications.

Figure 1 shows the schematic of fluorine/silver co-doped HA/TiO_2 nanotube coatings with antibacterial activity and

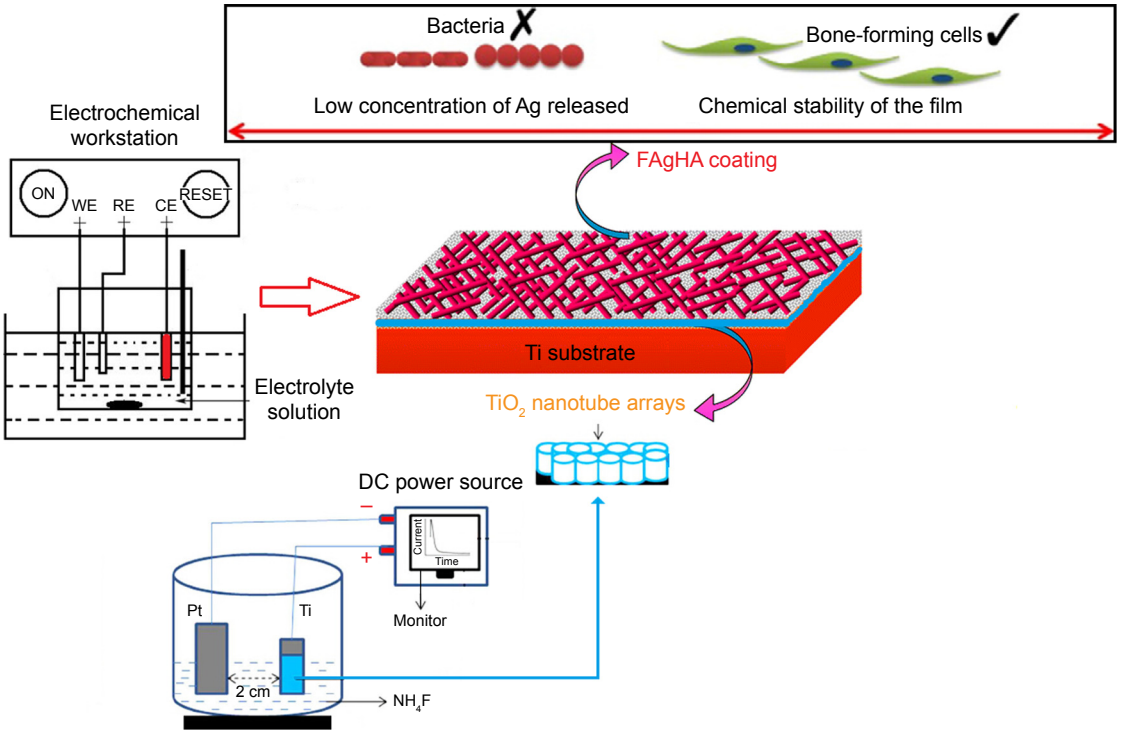

Figure 1 Schematic of silver- and fluorine-substituted hydroxyapatite/TiO_2 nanotube coatings with antibacterial activity and cytocompatibility fabricated by electrodeposition combined with anodization.

cytocompatibility fabricated by ED combined with anodization. The anticorrosion performance of the bilayer coating of the FAgHA and titania nanotubes (TNTs) on Ti within a simulated body fluid (SBF) solution was studied by electrochemical techniques. The antibacterial activity and in vitro cell viability studies have shown that the biological properties of the FAgHA/TNT-coated Ti are appropriate for orthopedic applications.

Materials and methods

Synthesis of TiO_2 nanotubes during the anodization process

A Ti foil with the dimensions of 10×10×1 mm^3 was embedded in epoxy resin such that an area of 1 cm^2 was exposed to the electrolyte; this foil was used as the substrate to grow TNT arrays. Silicon carbide papers of successively finer roughness were used to polish the surface to mirror quality. The Ti disks were cleaned with acetone, ethanol, and deionized water in an ultrasonic cleaner.[8] Then, they were etched in a solution of HF, HNO_3, and H_2O with the ratio of 1:4:5. The TNT arrays were prepared by the standard two-electrode anodization at room temperature in the potentiostatic mode. The cathode was a platinum plate, and the anode was the Ti sample. To create the nanotube layers, the samples were anodized in an electrolyte containing 0.5 wt% of HF solution.[22,26] The anodizing voltage was kept at 20 V during the 50-minute process. After anodization, the samples were ultrasonically washed in ethanol for 10 minutes to remove the fluoride ions remaining on the surface of the TiO_2 nanotubes.

Synthesis of FAgHA/TNT coatings

It was reported that the HA coating that was formed by the ED on the anodized Ti was not homogenous if the sample did not undergo any surface treatment.[21] To obtain a homogenous HA, the anodized Ti samples were treated by 2 M NaOH solution at 55°C for 3 minutes prior to ED. After the pretreatment, an HA coating was fabricated with ED at 60°C for 30 min – this HA coating was used as the control. A conventional cell was fitted with a platinum tablet as the anode and a Ti sheet, which was coated with the anodized TNT layer, as the cathode. The saturated calomel electrode (SCE) served as the reference electrode; an electrochemical workstation (CHI600E) was used for electrochemical measurements. A current density of 0.9 mA/cm^2 was used for the coating process. The concentration of the solution was kept uniform by using a magnetic stirrer that was controlled at 240 rpm. The electrolyte was prepared from the mixture of $Ca(NO_3)_2$ (0.021 mol/L), $NH_4H_2PO_4$ (0.025 mol/L), $NaNO_3$ (0.1 mol/L), and $AgNO_3$ (0.021 mol/L). The addition of $NaNO_3$ enhances the ionic strength. The molar ratios of

$Ag^+/(Ca^{2+} + Ag^+)$ were 0.5. The target (Ca + Ag)/P ratio of 1.67 was also designed. The pH value of the solution was adjusted to 4.5 by adding HNO_3 and $(CH_2OH)_3CNH_2$. The FAgHA coating was directly electrodeposited after adding NaF (1 mmol/L) into the electrolyte at 60°C±1°C. The concentrations of Ag and F were determined based on the previous studies.[26,27] After the ED procedure, the samples were sintered in air at 450°C for 2 hours. The purpose of the heat treatment was to enhance the crystallinity of the HA coating and to make the TNT transform from amorphous to anatase phase.[20] All of the reagents were of analytical grade and purchased from Aladdin (Shanghai Aladdin Biochemical Technology Co., Ltd., Shanghai, China).

Characterization of FAgHA/TNT coatings

The HA-coated Ti discs (n=3 for each analysis) were characterized for different properties as described. X-ray diffraction (D/Max-2500; Rigaku Corporation, Tokyo, Japan) equipped with the Cu-Kα radiation of λ≈1.5418 Å and 10°≤2θ≤70° was used for the phase analysis of the samples. The standards compiled by the Joint Committee on Powder Diffraction and Standards (JCPDS) were used for comparing the experimental X-ray diffraction profiles. The X-ray photoelectron spectroscopy (XPS) of the specimens were carried out by using a Thermo ESCALAB 250XI spectrometer. Fourier transform infrared spectroscopy (FT-IR; Nicolet 670, MA, USA) was used to evaluate the functional groups and structural changes of the milled samples. All spectra were recorded at the ambient temperature in the range of 4,000 to 400 cm^{-1}. The field emission scanning electron microscope (FE-SEM, JEOL JSM-7500F; JEOL, Tokyo, Japan) was used to examine the morphological features of the milled and annealed samples. The elemental compositions of the samples were measured with the energy-dispersive X-ray spectroscopy (EDS) that was attached to the FE-SEM. The bond strength between the FAgHA coating and the Ti substrate was examined with a universal testing machine (AG-10TA, Shimadzu, Kyoto, Japan) in accordance with the international standard of the American Society for Testing Materials (ASTM F1044-05).[28] A contact angle meter (Easy Drop Instrument, DSA 100; KRÜSS, Hamburg, Germany) was used to measure the wettability.[8]

Electrochemical behavior in the SBF solution

Potentiodynamic polarization test and electrochemical impedance spectroscope (EIS) in the SBF solution, which was prepared according to Kokubo's description,[29] were conducted to measure the corrosion resistances of the uncoated and HA-, and FAgHA/TNT-coated Ti samples. The samples were squares of the surface area of 1 cm^2 which were mounted on epoxy resin for electrochemical tests which were conducted with an electrochemical workstation (CHI600E) at 37°C in an open-air glass cell that contained 200 mL of Kokubo solution with the pH of 7.4. A three-electrode cell was used for the potentiodynamic polarization tests. A SCE, a graphite rod, and the sample itself were the reference, the counter, and the working electrodes, respectively. Prior to the electrochemical test, the open-circuit potential (OCP) was established by immersing the samples in the SBF for 30 minutes. The range of potentials and the scanning rate that were used for the potentiodynamic polarization tests were –0.8 to 0.5 V and 10 mV/s, respectively. The EIS were measured over the frequency range of 0.01 Hz to 100 kHz, and the data were analyzed by using ZsimpWin software.[6] To validate the reproducibility of the results, the electrochemical tests were duplicated.

Chemical durability and ion release tests

To examine the chemical durability and the ionic products of the FAgHA/TNT coatings, the coated samples were immersed in 10 mL of phosphate-buffered saline (PBS). The release medium was constantly shaken at 37°C for 1, 3, 5, 7, 9, 11, and 14 days. At the end of each immersing period, the inductively coupled plasma mass spectrometry (7700; Agilent Technologies, Santa Clara, CA, USA) was used to determine the concentration of Ag^+ and Ca^{2+} dissolved from the coating. The HA coating served as the control. The measurements were done in triplicate.

Antibacterial activity assay

Antibacterial properties of FAgHA specimens were investigated on gram-positive *Staphylococcus aureus* through quantity (bacterial counting) and quality (inhibition zone) assessments. The disk diffusion method was used for the qualitative evaluation.[30] The nutrient agar plates were inoculated with 1 mL of a bacterial suspension that included ~10^7 colony-forming units (CFUs)/mL of bacteria. The HA, AgHA, FHA, and FAgHA disks were gently placed on the inoculation plates and incubated at 37°C for 48 hours. The observed inhibition zone around each sample was recorded with a camera.

The bacteriological plate counting method was employed to evaluate the antibacterial ability of the HA, AgHA, FHA, and FAgHA coatings. The bacteria were cultured in the liquid nutrition agar medium at 37°C for 12 hours to the concentration of about 10^7 CFU/mL. All the laboratory supplies were sterilized in an autoclave at 121°C for 30 minutes. Briefly, 0.5 g of each sterile sample was dispersed in centrifugal tube

containing PBS (9 mL) and bacterial suspension (1 mL) and incubated at 37°C for 3, 6, 9, 12, 24, 36, and 72 hours. To count the bacteria, 100 µL of the suspension was then extracted from the centrifugal tube, was inoculated into the solid nutrition agar medium, and was then incubated for 24 hours at 37°C. The bacterial colonies were estimated according to the National Standard of China GB/T 4789.2; the antibacterial rates (R%) were calculated as 8:

$$R\% = (CFU_c - CFU_e) \div CFU_c \times 100$$

where the CFU_c represents the average number of the bacteria in the control group which is the bacterial suspension diluted by the PBS without adding any nanocrystal and the CFU_e represents the average number of the bacteria in the experimental group.

Mineralization in SBF

FAgHA/TNT-coated Ti was immersed in SBF for biomineralization. After immersed in 20 mL of SBF in sterilized bottle in a water bath at 37°C for 7 and 14 days, respectively, the specimens were washed with deionized water and dried under a vacuum. The FE-SEM equipped with EDS was used to characterize the surface morphology changes of the samples after the soaking in SBF.

Cytotoxicity evaluation

Cell culture

The mouse osteoblastic MC3T3-E1 cell line was purchased from the Type Culture Collection of the Chinese Academy of Sciences (Shanghai, China) (ATCC CRL-2594). The MC3T3-E1 was cultured in the a-MEM (Hyclone Laboratories Inc, South Logan, UT, USA) supplemented with 10% fetal bovine serum (Thermo Fisher Scientific, Waltham, MA, USA), 1% penicillin/streptomycin (Thermo Fisher Scientific), and 2 mM L-glutamine (Thermo Fisher Scientific); the culture was incubated in 5% CO_2 atmosphere at 37°C. Then, a volume of 250 µL of the MC3T3-E1 suspension at the density of 5×10^4 cells/well was seeded, and rested for 2 hours on the Ti foils in a 24-well plate forcell attached on Ti foil not dish. Then, 750 µL of the fresh medium was gently added along the wall of each wells. The MC3T3-E1 on the Ti foil was cultured in the medium for desired time points in all of the following experiments.

Cell morphology

After incubation for 24 hours, the adherent cells were fixed with 2.5% glutaraldehyde for 2 hours; they were then washed thrice with PBS for 5 minutes. Then, the dehydration of the samples was done with a graded series of alcohol for 15 minutes; thereafter, they were dried in supercritical CO_2.[7,8] The samples were then sputter-coated with gold, and the cell morphology was observed with the SEM. To observe the cytoskeleton, the adhering cells were immersed in a 4% paraformaldehyde solution for 10 minutes and were then stained with phalloidin (5 µg mL^{-1}; Sigma-Aldrich Co., St Louis, MO, USA). The fluorescence images of the adhering cells were obtained by a stereomicroscope (model SMZ745/745T; Nikon, Tokyo, Japan).

3-(4,5-Dimethyl-2-thiazolyl)-2,5-diphenyl-2-H-tetrazolium bromide (MTT) assay

MTT was purchased from Genechem (Shanghai, China). The MTT assay was used to measure cell vitality. At the prescribed time points, the Ti foils that had cells were gently rinsed with PBS and then transferred to a new 24-well plate. Then, 100 µL of the MTT solution (5 mg/mL) was added into a 24-well plate, and the samples were thereafter incubated at 37°C for 4 hours. Later, 500 µL of dimethyl sulfoxide was used to dissolve formazan, and the optical density (OD) was measured at 490 nm on the microplate reader.

Detection of intracellular alkaline phosphatase (ALP)

The osteogenic differentiation on the samples after 7 and 14 days of culturing was determined by using an ALP assay. The medium was removed, and 500 mL of Triton X-100 (1%) was added into the 48-well plates. After being shaken for 5 minutes, the 24-well plate with the samples was incubated in a water bath at 37°C for 1 hour. Then, the microplate reader was used to test 30 mL of the supernatant with an ALP ELISA kit at the wavelength of 520 nm.

Results and discussion

Characterization of TN

Figure 2 shows the top and cross-sectional FE-SEM micrographs of the anodized surface of Ti. As shown in Figure 2A, the TiO_2 nanotubes grow perpendicular to the surface of the anodized sample; the total thickness of the nanotube layer is about 400 nm (Figure 2B); the average wall thickness of the nanotubes is 15 nm, and their average inner and outer diameters are 100 and 130 nm, respectively (Figure 2C). Figure 2D shows the FT-IR spectra of the anodized surface of Ti. The band at 685 cm^{-1} is assigned to the vibrational mode of bending of Ti–O bond.[8] The curved surfaces of the nanotubes provide a large number of active sites that are available for nucleation, which consequently results in

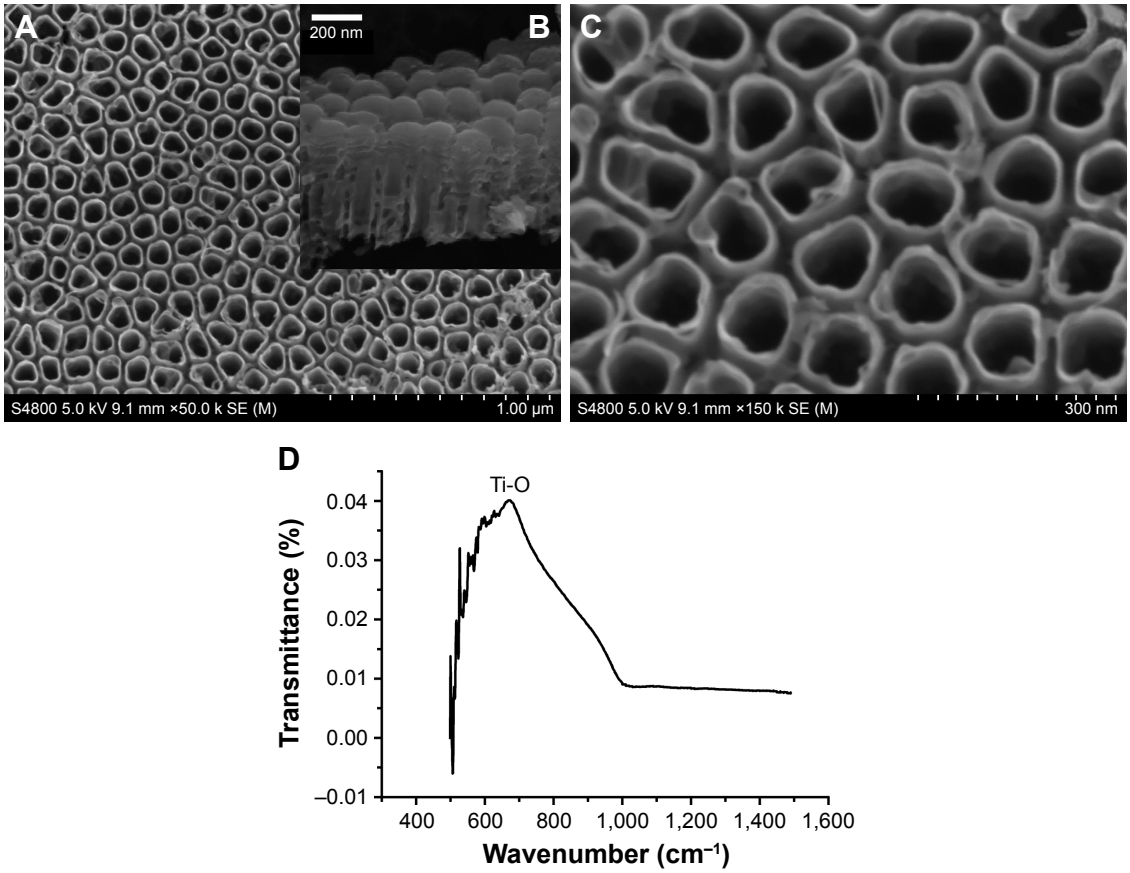

Figure 2 FE-SEM images of TiO_2 nanotubes (**A** and **C**) and cross-section (**B**), FT-IR spectra of TiO_2 nanotubes. (**D**) FT-IR spectra of the anodized surface of Ti.
Abbreviations: FE-SEM, field emission scanning electron microscope; FT-IR, Fourier transform infrared spectroscopy.

a faster growth of the HA crystals – which then translates into a high surface coverage.[20]

Characterization of as-deposited coatings

Figure 3A compares the XRD patterns of Ti after the HA/TNT deposition and the FAgHA/anodized double-layer fabrication. Both the coatings were annealed to 450°C since the as-deposited coatings are amorphous. The peaks from both the coatings are in line with the HA pattern (JCPDS No 09-0432). The peak related to the [002] plane of the HA crystal that happens at 25.9° of the FAgHA/TNT XRD pattern is higher than that of the HA coating, suggesting that the nano-rod-like crystals prefer to grow along the c-axis which is [001] direction.[14] It is noteworthy that the XRD patterns of

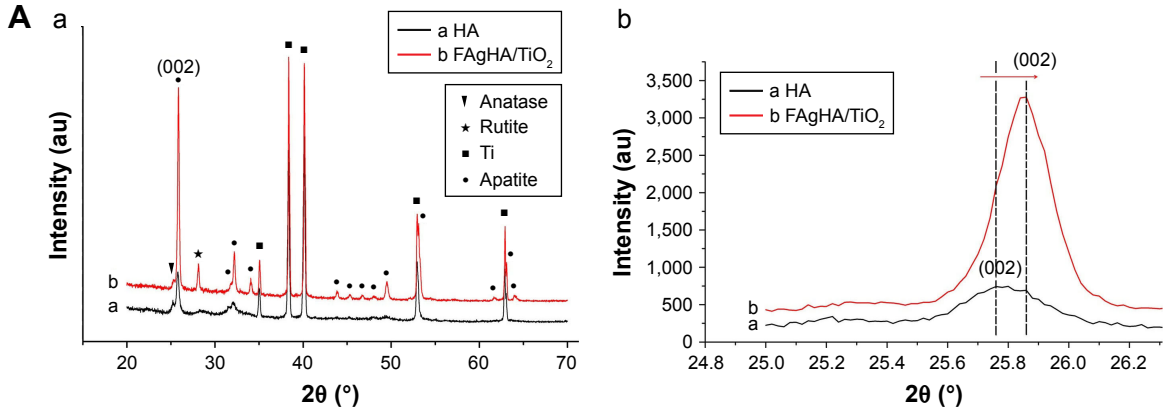

Figure 3 (*Continued*)

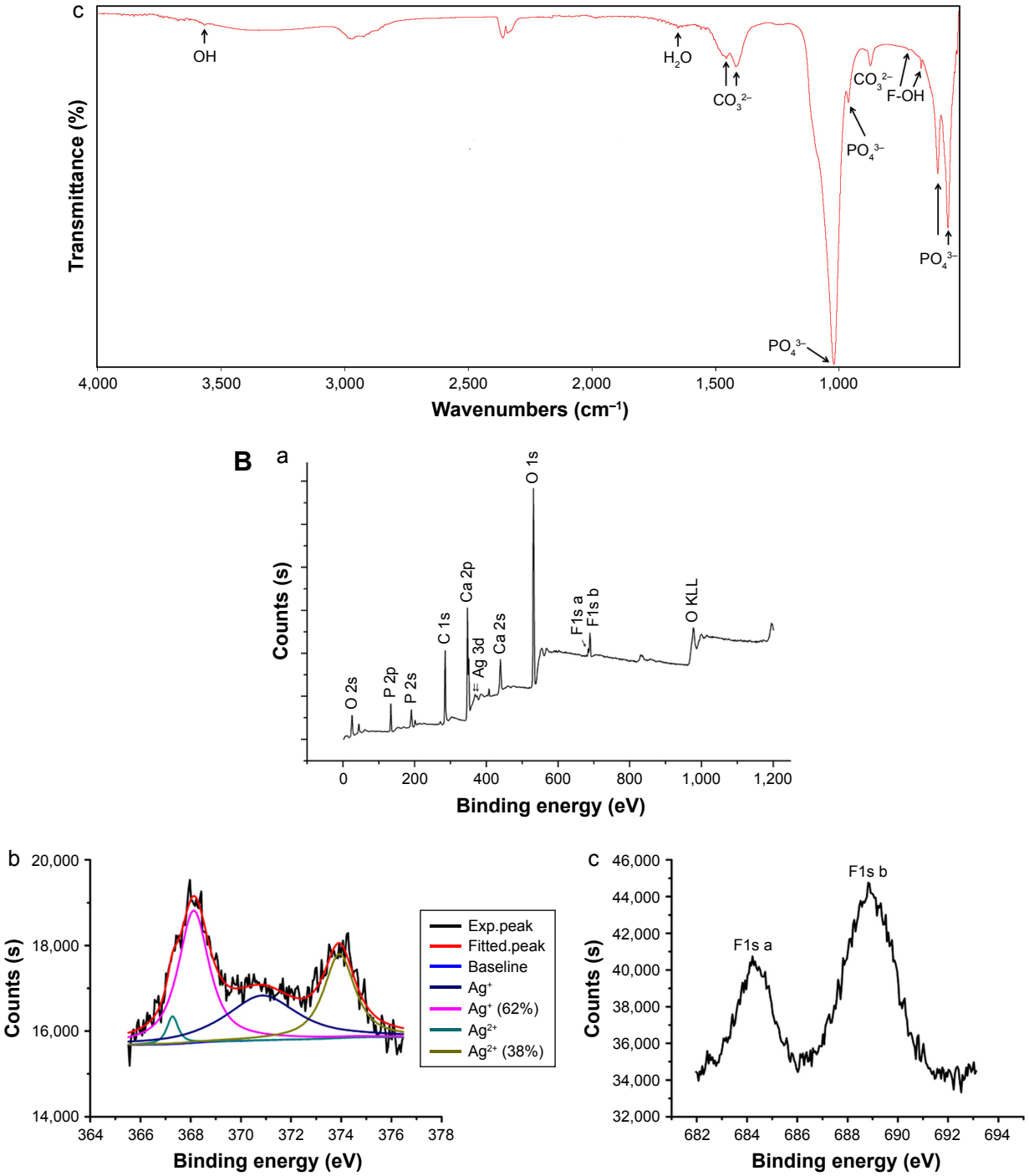

Figure 3 (**A**) XRD pattern of the (a) HA coating on CP-Ti and the (b) FAgHA coating on Ti; FT-IR spectra of Ti coated with FAgHA (c). (**B**) XPS general spectrum of FAgHA coating (a), F (1s) (c), and deconvolution of Ag (3d) XPS peak b.

Abbreviations: XRD, X-ray diffraction; HA, hydroxyapatite; FT-IR, Fourier transform infrared spectroscopy; XPS, X-ray photoelectron spectroscopy; FAgHA, F-and-Ag-substituted HA.

the FAgHA exhibit higher crystallinity than those of the HA coating. The XRD patterns of the HA and FAgHA coatings did not show any significant amorphous background hump. Moreover, no other Ca-P phases were detected in the XRD patterns of the coatings. The patterns show anatase TiO_2 phase which can be due to the heat treatment at 450°C that involves the amorphous-to-anatase phase transformation.[28] The XRD peaks for crystallized TiO_2 were observed at 2θ =25.5° and 27.58°, which are related to anatase (JCPDS card no: 21-1272) and rutile phases (JCPDS no: 21-1276), respectively.[31]

The diffraction peaks of the FAgHA/TNT coating were at 2θ values that were slightly higher than those in the standard

pattern of the HA, which may be attributed to the crystal lattice distortion due to the substitution of Ag^+ and F^- ions into the HA lattices (Figure 3A(b)).[26,27] Ag^+ incorporation into the HA leads to a slight increase in the diameter of the spheres of doped HA. As compared with the HA, the incorporation of Ag^+ into the HA shifts the diffraction peaks to lower 2θ values, which indicates an expansion in the crystal lattice, which can be attributed to the larger ionic radius of Ag (0.126 nm) compared with Ca (0.099 nm).[32] On the other hand, the incorporation of F^- into the HA moves the major peaks of the HA to higher 2θ values, confirming that some of the fluoride ions are substituted for the hydroxyl group of the HA.[25] Then, the co-addition of Ag and F into the HA has moved the diffraction peaks to higher 2θ values, which indicates that the lattice parameters have been reduced (Figure 3B); that is, F^- has had a bigger effect than Ag^+ in changing the unit cell of the HA crystal.[13] This shift of the XRD peaks (Figure 2B) with respect to the F/Ag-free HA served as an evidence of F/Ag co-substitution in our fabricated coatings.[15] However, the aforementioned peak shift might be due to the strain effects and/or the mismatch between the thermal expansion coefficients of the film and the substrate.[4]

Figure 3A(c) shows the FT-IR spectra of the FAgHA nanocoating. The two bands at 3,442 and 1,638 cm^{-1} belong to the vibration of the adsorbed water in apatites. The vibrations that are related to the phosphate groups were detected by the bands at 567 and 603 cm^{-1} (ν_4), 962 cm^{-1} (ν_1), and 1,041–1,087 cm^{-1} (ν_3).[6,33] The presence of three bands at around 877 cm^{-1} (ν_2), 1,421 cm^{-1} (ν_3), and 1,457 cm^{-1} (ν_3) were due to carbonate vibrations, revealing some substitution of PO_4^{3-} sites by CO_3^{2-} ions.[33] The band 3,571 cm^{-1} is related to the symmetrical stretching (ν_1) mode of the OH^- in the HA.[13] Based on the classical review of Fowler,[34] the shift of the FT-IR spectrum in the FAgHA film to 3,543 cm^{-1} is attributed to the partial substitution of F^- for OH^- in the HA structure. It has also been shown that the substitution of F^- for OH^- in the HA ($Ca_{10}(PO_4)_6F_{2-x}(OH)_x$) shifts the OH^- band at 630 to 670 cm^{-1}.[34] The FT-IR spectrum of the FAgHA sample, shown in Figure 3A(c), includes two OH^- bands at 742 and 676 cm^{-1}.[15] Confirming the substitution of F^- for OH^-, the subsequent shifts in the HA spectrum suggests that the FAgHA/TNT structure had regions of high fluorine concentrations.[13] The FT-IR spectra did not show any indication of Ag–O bonding from the Ag_2O or AgO phases, which indicates that Ag^+ was indeed incorporated into the HA structure.[8]

XPS is another effective way to identify the Ag^+ and F^- incorporation into the HA structure. The XPS results for the FAgHA/TNT coatings have been highlighted in Figure 3B(a). The peaks corresponding to Ca2s (438.7 eV), $Ca2p_{3/2}$ (347.5 eV), $Ca2p_{1/2}$ (351.1 eV), P2s (191.1 eV), O1s (531.6 eV), F 1s a (684.2 eV), F 1s b (688.3 eV), $Ag3d_{5/2}$ (368.0 eV), $Ag3d_{3/2}$ (373.9 eV), and O2s (23.0 eV) are all obviously evident. The peaks corresponding to Ca2s, $Ca2p_{3/2}$, $Ca2p_{1/2}$, P2s, O1s, and O2s are clearly observed in line with previous reports.[35,36] The presence of an F 1s peak in the XPS spectrum is an indication of the bonding of fluorine to the film surface (Figure 3B(c)). The fitting of the F 1s envelope revealed the presence of a main peak at 688.3 eV and a minor contribution at 684.2 eV. The energy at 688.3 eV corresponds to the fluoride ions interacting with calcium atoms in the structure of fluorapatite (FA).[37] This binding energy of fluorine and calcium (F-CaII) is an indication of the partial substitution of hydroxyl by fluoride ions in the HA structure. As reported previously,[38] the fingerprint of F in the FHA is the low-intensity F 1s peak at 684.2 eV. The peaks of Ag (($3d_{5/2}$) 368.0 eV) and Ag (($3d_{3/2}$) 373.9 eV) are in agreement with the previously reported values.[8] Furthermore, the splitting of the 3d doublet of the Ag at 6.1 eV demonstrates the existence of Ag ions. Figure 3B(b) shows the XPS narrow scan spectra of the Ag element. The binding energies of the Ag ($3d_{5/2}$) core level for Ag_2O and AgO are 368.2 and 367.7 eV, respectively.[26] Hence, based on the deconvolution of the Ag ($3d_{5/2}$) peak into two Gaussian components with similar full-widths-at-half-maximum after Shirley background subtraction, we found that ~38% of the incorporated silver was in the Ag^{2+} chemical state, and the rest of the silver was incorporated into the HA as Ag^+ state. The XPS results further confirm the successful incorporation of the Ag^{2+}/Ag^+ in the FAgHA/TNT coating. No other elemental species were detected at least at the detection limits of the instrument (~0.1 atomic % concentration).

Figure 4 shows the FE-SEM microstructure information of the HA and FAgHA/TNT coatings on Ti along with the cross-sectional image of the as-formed bilayer coating. The surface of the HA has a micro-flake-like structure with many agglomerated features (Figure 4A and B). In biological environments, the body fluid will infiltrate into the pores, and induce the fast corrosion of the substrate. The loose microstructures on the surface are comparatively easy to shed, which may result in inflammation during implantation periods.[39] Morphologies of modified HA layers have significantly been changed compared to the pure HA layer. By contrast, the FAgHA/TNT coating shows compact dandelion-like aggregates of acicular-shaped crystals (Figure 4D), which densely and uniformly cover the entire surface of the TNTs without any apparent defects

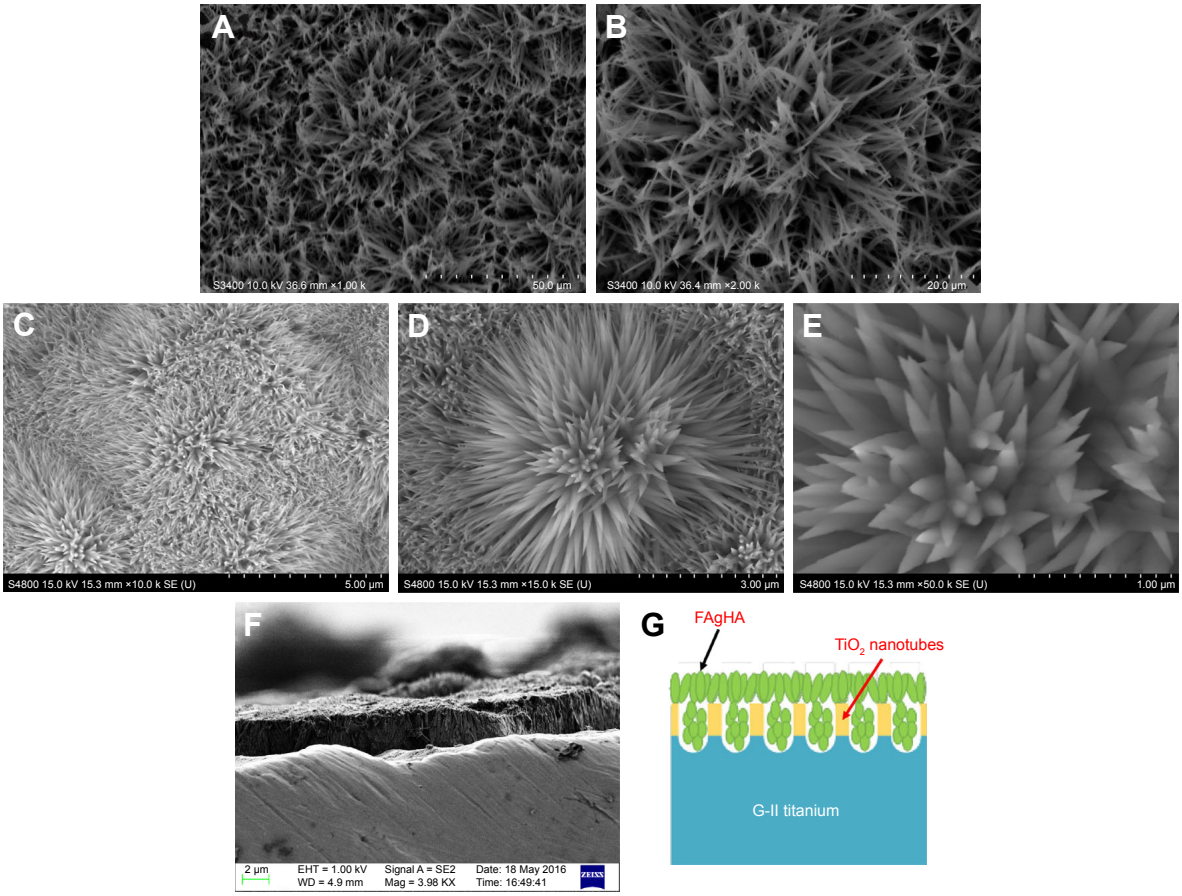

Figure 4 SEM image of HA coating (**A** and **B**) (low magnification and high magnification); SEM images of FAgHA coatings (**C**–**E**) (low magnification and high magnification); cross-section morphology of the FAgHA coating on TNT (**F**); the schematic diagram of cross-section of the FAgHA coating on TNT (**G**).
Abbreviations: SEM, scanning electron microscope; HA, hydroxyapatite; TNT, titania nanotube; FAgHA, F-and-Ag-substituted HA.

(Figure 4C). The diameter of the acicular-shaped crystals ranges from 30 to 50 nm (Figure 4E), which is similar to that of natural bones.[25] Importantly enough, an artificial material that is more similar to the tissue structure can more effectively support the natural healing process.[20] Compared to the flake-like HA coating, the FAgHA/TNT acicular-shaped coating can better protect the substrate, thanks to its dense and uniform structure; the acicular-shaped coating provides more contact area with the surrounding fluid after the implantation and is therefore more favored for the deposition of apatite. Consisting of positive Ca and negative PO_4 ions, and the closely packed OH and F groups, the FAgHA nanostructure has played an important role in crystallization and bone bonding.[25] Moreover, the nano-sized HA is more effective in bone cell adhesion and proliferation.[40] Figure 4F presents the cross-sectional FE-SEM images of the FAgHA-modified nanotubular Ti. The FAgHA/TNT coating is of a thickness of about 2–3 μm and there is a sound adhesion to the underlying substrate – the coating can tightly adhere to the substrate.

Figure 4G presents the schematic diagram of the coating section. The FAgHA coating is embedded in the interior and the surface of the nanotube. A significant increase in FAgHA/anodized adhesion strength may be achieved due to the interlocking of the roughened surface with the FAgHA colloidal particles which penetrated into the voids of the TiO_2 nanotubes.[40] In addition, the effect of the NaOH pretreatment on crystal size of electrodeposited HA was previously described by Oh et al.[41] In that study, the growth of finer-scale structure of HA from a nanostructured substrate (TiO_2 nanotube arrays) is one way to fabricate nanostructured HA coating for orthopedic implants.

The elemental composition of the FAgHA has been given in Figure 5A. According to the EDS spectrum, the sample mainly consisted of F, Ag, Ca, P, O, and C; components P, O, Ca, and C are primarily derived from the carbonated HA, whereas Ag and F elements may originate from the substitution of Ca^{2+} ions in the HA crystal lattice by Ag^{+} and OH by F.[16] The only by-product of the milling of the sample was water, and no other chemically stable contaminant was

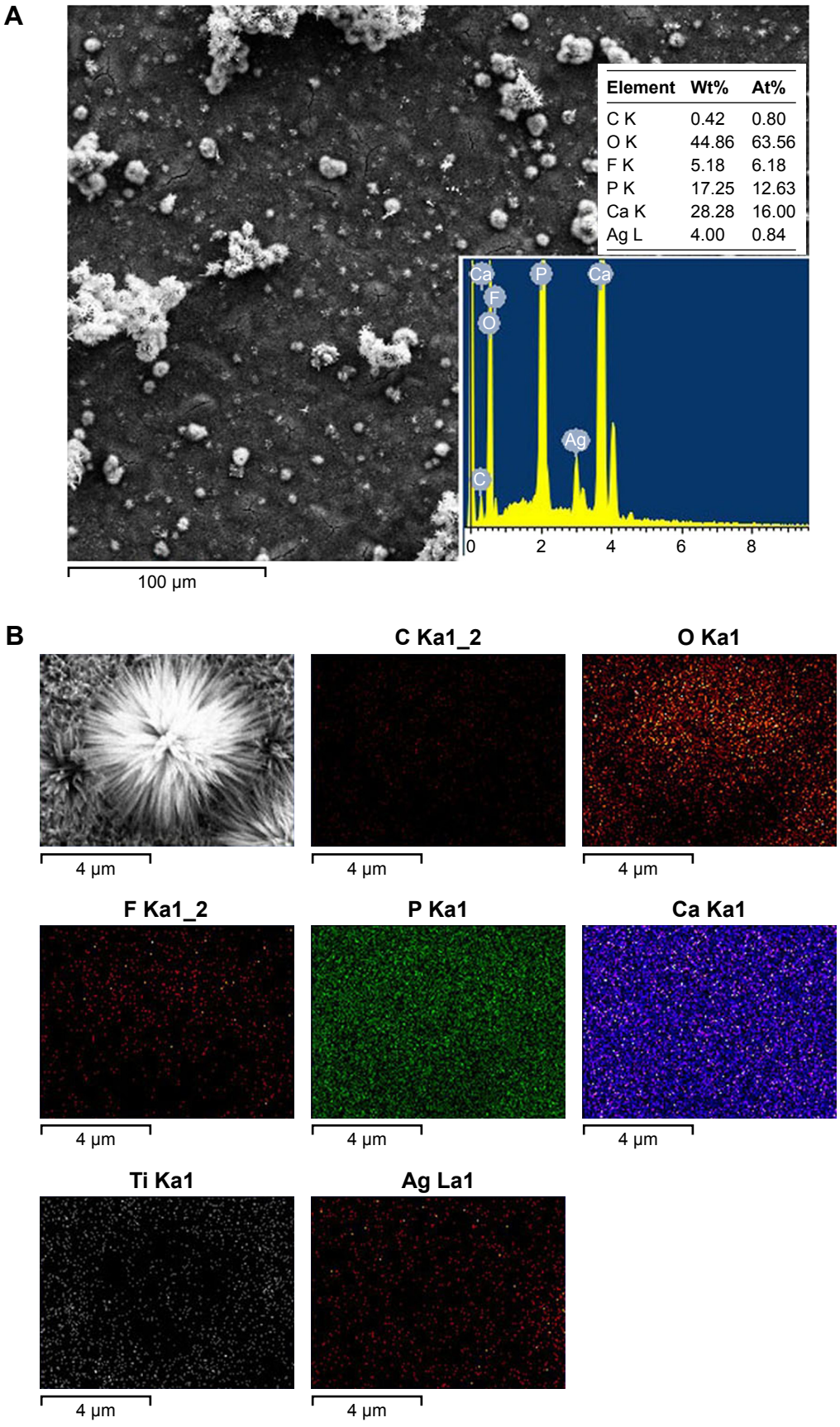

Figure 5 EDS mapping spectrum (**A**) and EDS spectrum (**B**) of the FAgHA coating.
Abbreviations: EDS, energy-dispersive X-ray spectroscopy; FAgHA, F-and-Ag-substituted HA; HA, hydroxyapatite.

therefore observed. The decrease of the (Ca+Ag)/P atomic ratio from 1.67 – the theoretical HA stoichiometry – to 1.27 in the FAgHA layer is in good agreement with the replaced amount of Ca ions by Ag ions. The outer FAgHA coating is composed of calcium-deficient HA, which may cause excellent biodegradation and induce the precipitation of bone-like apatite after implantation.[8] The distribution of F and Ag into the deposited layer was evaluated with the EDS mapping of the elements which has been shown in Figure 5B. The mapping shows a uniform distribution of the elements throughout the surface layer.

Bonding strength

The bonding strength of the deposited HA with the Ti substrate was 8.8±3 MPa. The adhesive strength of the AgHA coating to the Ti substrate was calculated at 8.2±3 MPa; the FAgHA/Ti and FAgHA/TNT adhesion were 12.2±4 and 17.1±5 MPa, respectively – the incorporated F have drastically enhanced the adhesion of the coating to the Ti substrate,[28] which can be understood as follows. The coefficients of thermal expansion (CTE) of the materials involved in the coating are 8.9×10^{-6} K^{-1} for Ti6Al4V, $12.7–13.5\times10^{-6}$ K^{-1} for the HA, and $8.5–9.1\times10^{-6}$ K^{-1} for FA – $Ca_{10}(PO_4)_6F_2$ where F substituted all the OH in the apatite structure.[42] Performing scratch tests, Cheng et al found that the highest peeling-off value for the FHA coatings is 478 mN (adhesive failure), which approximately equals a pull-out strength of 20 MPa.[42] Moreover, commercial plasma-spray coatings reached ~20 MPa of the bonding strength.[43] The CTE value of the FAgHA can be reasonably assumed to be between those of the HA and FA. This CTE mismatch between the coating and the substrate develops a residual stress that is proportional to the CTE difference.[42] The incorporation of F reduces the CTE mismatch, and consequently, the reduced residual stress makes the bonding of the coating to the substrate stronger. The highest adhesion of 17.1±5 MPa of the FAgHA/anodized Ti sample can thus be attributed to the interlocking of the roughened surface with the FAgHA colloidal particles which penetrated into the voids of the TNT.[28,44] The superior chemical bonding of TiO_2 to the substrate improves the interfacial cohesion in the FAgHA/anodized double layer.[28] Parcharoen et al showed that the TNT arrays can improve both the adhesion of electrodeposited HA and the osteoblast cell growth.[21] Reportedly, the surface morphology of the TNT promotes the mechanical interlocking between the HA coating and the TiO_2.[22,45]

Corrosion behavior

Tafel polarization curves of bare Ti and Ti coated with bioceramics were recorded for comparing the degradation rates. The Tafel curves were evaluated by a linear extrapolation of the anodic and cathodic slope at ±100 mV from OCPs. Figure 6A shows the polarization curves of the bare and the coated substrates along with the obtained electrochemical parameters of the samples. The corrosion potential (E_{corr}) and current density (i_{corr}) of the HA-coated sample in comparison with the bare sample have shifted from −551 mV and 3.71 µA to −489 mV and 0.57 µA, respectively. A higher corrosion potential and lower corrosion current indicate a higher corrosion resistance.[1,6] Moreover, as seen in Figure 6A,

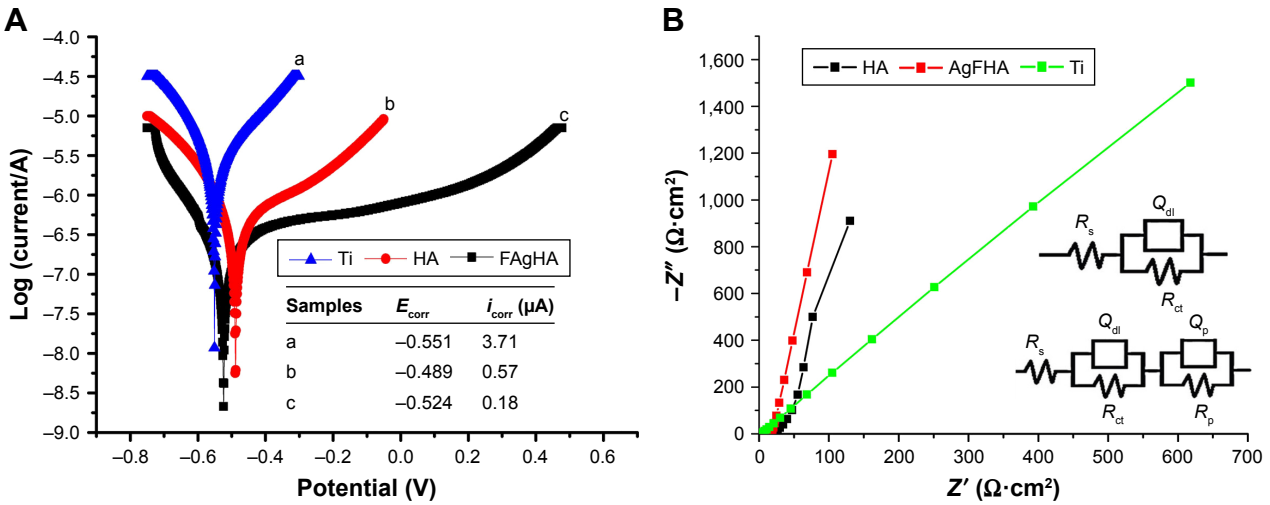

Figure 6 (**A**) Tafel polarization curves of bare Ti and Ti coated with bioceramics. (**B**) Experimental and fitted Nyquist plots of bare Ti and Ti coated with bioceramics, equivalent electrical circuit for EIS data fitting for bare Ti and the Ti coated with bioceramics.
Abbreviations: EIS, electrochemical impedance spectroscope; HA, hydroxyapatite; FAgHA, F-and-Ag-substituted HA.

the co-incorporation of F and Ag into the HA shifts the E_{corr} and i_{corr} of the coated substrate from −551 mV and 3.71 µA to −524 mV and 0.18 µA, respectively. The uniformly compact surface of the FAgHA/TNT coating can better protect the substrate, which prevents corrosive ions from entering into the substrate.[1,2] Electron and ion transports at the coating/electrolyte interface are hindered by the FAgHA coating deposited on the protective TiO_2 nanotubes layer whose regeneration can also be promoted by the coating through its uncompressed structure, which then protects the substrate against corrosion.[4]

Very useful information about the resistive and capacitive behavior of all as-coated samples can be obtained by the EIS.[2] The Nyquist plots of the uncoated Ti, HA-coated, and FAgHA/TNT-coated Ti samples in the SBF solution at the OCP conditions have been shown in Figure 6B. As can be seen, the coated and uncoated samples showed a single capacitive loop at all high frequencies; compared with the loops of the uncoated Ti, those of the bi-layered FAgHA/TNT and the monolayered HA coatings have significantly larger diameters. This phenomenon makes it difficult to separate the time relaxation of the physical impedance of the coating from that of the electrochemical reaction impedance at the Ti/coating interface.[1,2] The same conclusion can be reached by qualitatively comparing the polarization data with the results pertinent to the Nyquist plots.

Based on the EIS data, Figure 6B manifests an equivalent circuit model between the corroded samples and the SBF solutions. The impedance spectra were further fitted with an equivalent circuit by using ZSimpWin software with the $Rs(Q_{dl}R_{ct})$ model for the uncoated Ti, where Rs is the resistance of the electrolyte; R_{ct} is the polarization resistance of the passive layer on the CP-Ti substrate, and Q_{dl} is the double-layer capacitance of the interface of the passive layer and the electrolyte. $R_s(Q_pR_p)(Q_{dl}R_{ct})$ model was used to simulate the corrosion behavior of the FAgHA/TNT-coated Ti. R_s, R_p, Q_p, R_{ct}, and Q_{dl} are the resistance of the solution, the resistance of the coating, the capacitance of the coating, the charge transfer resistance, and the capacitance of the double layer, respectively. The FAgHA/TNT coating possesses the highest corrosion resistance.

Chemical durability and ion release tests

Figure 7 shows the chemical stability and ion release of the FAgHA/TNT coating in the PBS. The Ca ion concentration in the pure HA is higher than that in the FAgHA/TNT coating, which indicates that the pure HA coating has a higher dissolution rate. This can be put down to the higher density and chemical stability of the FAgHA/TNT coating – the higher release of Ca ions from the pure HA is due to its lower chemical stability as shown in Figure 7A. The contraction in the a-axis of the crystal lattice of the FAgHA because of the incorporation of F enhances its crystallinity and stability,[15] which consequently reduces its solubility.[13]

Figure 7B shows the effect of the immersion time on the amount of Ag^+ released in the PBS. The Ag^+ release from the FAgHA/TNT was very fast in the first 5 days, which then gradually decreased in the following days. Therefore, the FAgHA/TNT-coated Ti implants continuously release Ag^+, resulting in a high enough initial concentration of antimicrobial agents (Ag^+). This can prevent bacterial adhesion to implants after the implantation surgery.[12] Moreover, a continuous release of Ag^+ after the implantation surgery is also very essential to prevent the formation of a bacterial

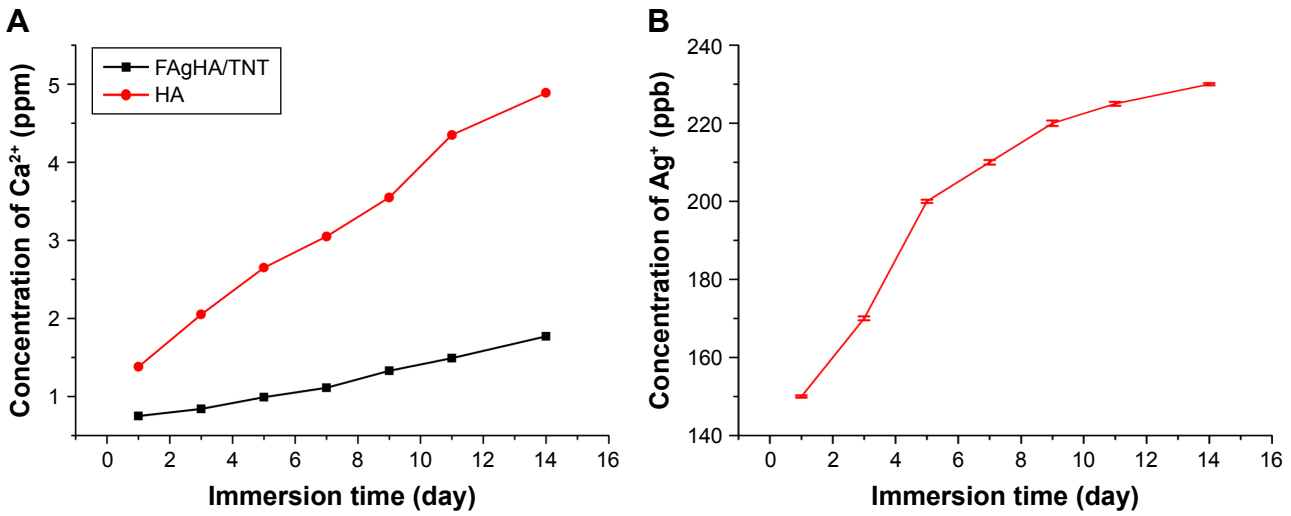

Figure 7 Amount of calcium (**A**) and silver (**B**) species delivered per surface area released from the FAgHA coating under static incubation at 37°C in PBS.
Abbreviations: PBS, phosphate-buffered saline; HA, hydroxyapatite; FAgHA, F-and-Ag-substituted HA.

biofilm on Ti-based metallic implants.[46] In view of the cytotoxicity of Ag^+ ions, their concentration should be controlled so optimally that any potential side effects are prevented. The amount of the Ag^+ released from our fabricated FAgHA/TNT coating was 230 ppb, lower than the maximum toxic concentration of 300 ppb in human blood – therefore, the FAgHA/TNT coating can be a noncytotoxic biomaterial.[47]

Antibacterial efficacy

To evaluate the bactericidal effect, we cultivated the bacteria with various samples according to the bacteria counting method. Figure 8A–E summarizes the results of the antimicrobial properties of HA, FHA, AgHA, and FAgHA composites against *S. aureus* with an exposed time of 24 or 36 hours. Compared with the blank and HA groups, the Ag-doped HA groups allow for very low proliferation of bacteria, implying the apparent bacteriostatic effect on *S. aureus*. Compared to the pure apatites, the Ag-modified apatites (AgHA or FAgHA) strongly affected the viability of the bacteria (pattern vs clear bars in Figure 8F). The reduction ratio of viable cells in the AgHA was about 99.5% or 100% ($p<0.05$) for 24 or 36 hours of incubation, respectively (Figure 8G). Interestingly, regardless of the time of

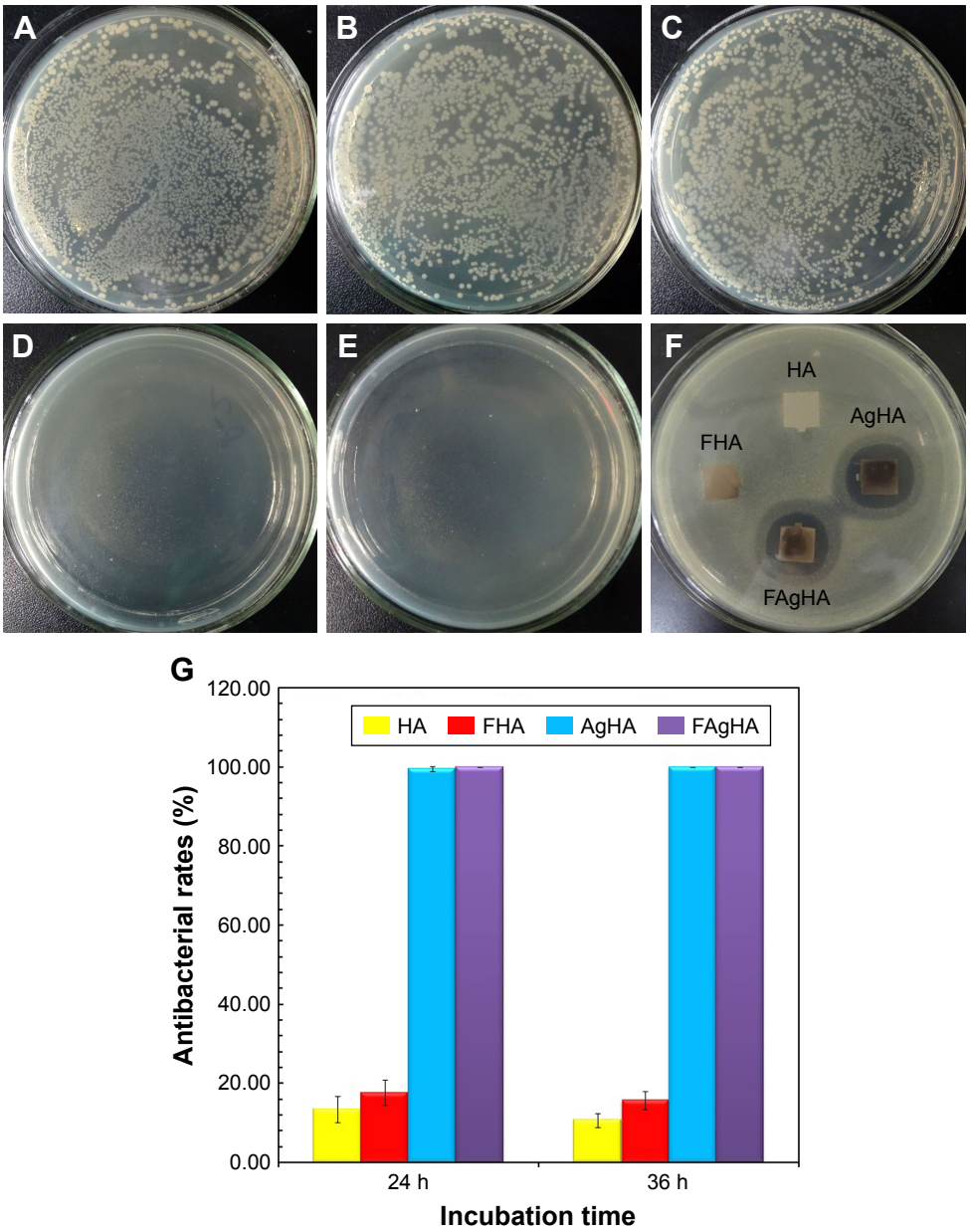

Figure 8 Representative macroscopic images of viable adherent *Staphylococcus aureus* on different experimental material surfaces: (**A**) witness test; (**B**) HA; (**C**) FHA; (**D**) AgHA; (**E**) FAgHA; (**F**) zone of inhibition test results of HA, FHA, AgHA, and FAgHA against *S. aureus*; and (**G**) antimicrobial rates of FAgHA.
Abbreviations: HA, hydroxyapatite; FAgHA, F-and-Ag-substituted HA; FHA, fluorhydroxyapatite.

incubation, silver-modified FA showed 100% inhibition of bacteria proliferation ($p<0.05$). Some cell reduction was also observed for the HA and FHA without silver ions – microorganism cells can somehow adhere to the particles of HA, which may add to the total number of cells reduced by the tested samples.[4] The bactericidal activity was therefore dependent on the type of apatite, and the silver doping of the FAP could drastically increase the antibacterial effects. Moreover, the possibility of bacteria adhesion to the FAgHA can explain its higher efficacy of antibacterial activities. In summary, no viable bacteria were identified for any of the silver-modified composites, confirming their strong antibiofilm activity.

Figure 8F shows the antibacterial activity of HA, AgHA, FHA, and FAgHA coatings against *S. aureus*. The HA does not show antibacterial activity – the whole HA is surrounded by the attached *S. aureus* cells. Moreover, the FHA sample also does not show any antibacterial activity. However, the AgHA and FAgHA coatings show a clear bacterial inhibition zone for *S. aureus*. Interestingly, the sizes of the inhibition zones of the AgHA are a little larger than those of the FAgHA, which can be attributed to lower release of Ag^+ due to the lower dissolution rate of FAgHA.

Physical and chemical characteristics of materials such as morphology, surface properties, and chemical composition can affect the viability of microorganism.[48] It has been demonstrated that the nanostructure with a homogeneous high-surface-area nano-rod-like structure can promote the antibacterial activity through undermining the bacterial cell membrane.[49] However, we have not found any antibacterial effects for the FHA nanocrystal surface; therefore, the antimicrobial effect should be attributed to the release of silver ions in the FAgHA coating.[50] Binds to proteins on the cell membrane, the released Ag^+ causes structural changes and damages to the membrane.[51] Then, the Ag^+ penetrates into the cell and causes bacterial death through interacting with nucleic acids.[52] The effective antibacterial activity at Ag^+ concentrations was of as high as 35 ppb.[53,54] As the total amounts of the released Ag^+ (150 ppb) were >35 ppb, the FAgHA reduced the bacteria by 100% in 24 hours of incubation; that is, the initial concentration of the Ag^+ released by the FAgHA is high enough.

Static contact angle

The contact angle was measured by using a classic contact angle meter. For all the samples, the contact angles are <90°, except for the sample shown in Figure 9A(d) which exhibits a hydrophilic behavior which is directly linked with the biocompatibility – the lower the contact angle is, the more biocompatible the material is.[3] Figure 9A presents all the values obtained for all the samples. Sample c with the contact angle of 26.9°±1.8° is the most hydrophilic sample, for the HA is porous and very biocompatible. The less hydrophilic sample is sample a (Ti) with the contact angle of 71.1°±10.2°. Almost all the samples, including the TiO_2 nanotubes (75.2°±11.4°) are within a hydrophilic domain – the contact angles are <90°. It is noteworthy that the most hydrophobic sample is sample d (FAgHA/TiO_2) with the contact angle of 110°±18.2°, which can be put down to the dandelion-like aggregates of needle-shape nanocrystals at the surface of FAgHA/TiO_2. Although the FAgHA/TNT nanocomposite is hydrophobic, previous studies have shown that the activity of integrins is potentially favored at a nanoscale surface; integrins induce cell adhesion and spreading, or cell migration, growth, and differentiation.[55]

In vitro bioactivity

The definition of the bioactivity of ceramics marks the ability of bonding with the host bone tissue.[33] The in vitro bioactivity is assessed by examining the growth of a bone-like apatite on the surface of the sample after soaking in Kokubo's SBF solution. Figure 9B(a–f) presents the SEM micrographs of the surface of FAgHA. After 7 days of immersion, a newly formed layer with a typical spherical shape covered the surface of the sample (Figure 9B(a–c)); the EDS analysis showed that this layer was chemically similar to apatite. Figure 9B(d–f) shows the apatite formation on the surface of partially Ag^+-and-F^--substituted HA after soaking in the SBF for 14 days. As seen, numerous tiny crystals precipitate on the surface of the sample as apatite clusters that densely cover the entire surface of the sample. Note that different observations on the apatite layer growth on the surface of the samples are relevant to their morphologies, which is in line with previous findings.[56,57] Moreover, the EDS spectra shown in Figure 9B(g) shows the existence of Mg, Na, O, Ca, P, and Cl; the Cl and Na can be attributed to the NaCl precipitated from the medium, and the Ca and P are due to the apatite layer (Figure 9B(g)). The fact of the apatite formation on the FAgHA indicates that the Ag^+ and F^- incorporation into the HA structure induces a good bioactivity – the FAgHA could be potential bioactive ceramics.

Cell morphology

Figure 10 shows the SEM results of the cells adhered on the bare and coated Ti substrates after 1 day of incubation. The cells attached and started spreading very well on the

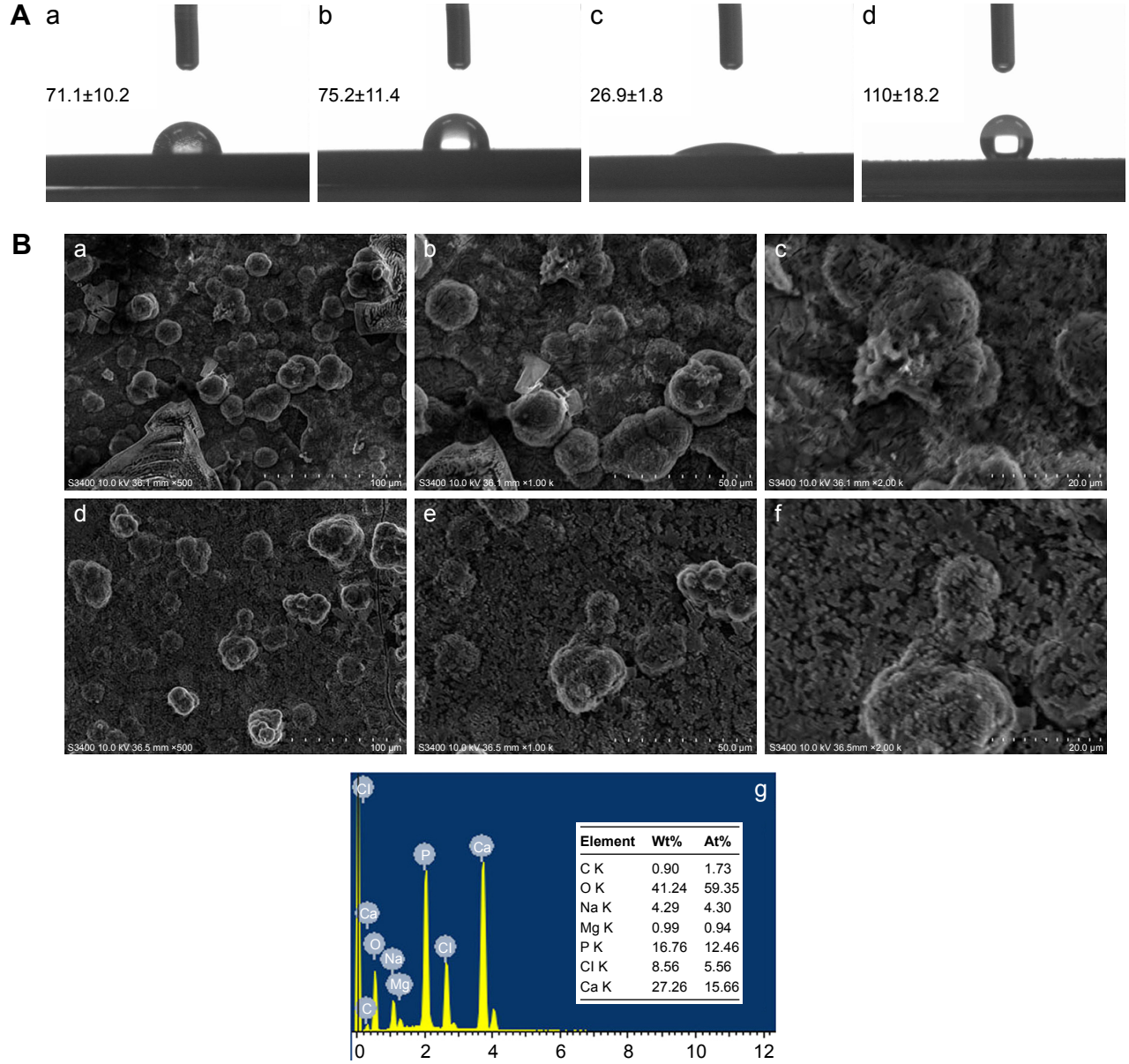

Figure 9 (**A**) Water droplet images and corresponding contact angle values of (a) Ti, (b) nanotube-formed Ti, (c) HA coating, and (d) FAgHA coating. (**B**) SEM images of the FAgHA coatings after immersion in SBF for 7 days (a–c) and 14 days (d–f); (g) EDS elemental spectrum of the FAgHA coating after immersion in SBF for 14 days.
Abbreviations: HA, hydroxyapatite; SEM, scanning electron microscope; EDS, energy-dispersive X-ray spectroscopy; SBF, simulated body fluid; FAgHA, F-and-Ag-substituted HA.

Ti, HA, and FAgHA substrates as shown in Figure 10A–F, respectively. Similar spread-shaped MC3T3-E1 was observed on the three coating surfaces. MC3T3-E1 cells shows a typical osteoblast phenotype, which appears three-dimensional (3D) and flattened with numerous filopodia and lamellipodia extensions. Meanwhile, the initial cell adhesion and spreading activity of the MC3T3 that was seeded on the samples was studied by fluorescence microscopy. Cytoplasmic actin skeletons are visualized through FITC-phalloidin staining (Figure 10G–I). The cells grown on the Ti substrate show a normal morphology – a well-organized actin cytoskeleton with numerous cell–cell contacts. The osteoblasts cultivated on the surface of the HA/TiO_2 sample were well-spread and presented a strong cortical actin staining and filopodial extensions. As revealed by the SEM image (Figure 10B, D, and F) and green fluorescence of FITC, the surface topography clearly controlled the cell attachment and spreading. The cell alignment followed the pattern of the surface texture which was not flat and induced a 3D arrangement of osteoblasts. Such an alignment was also observed for the FAgHA/TNT sample which provided a nano-composite scaffold for a 3D culture

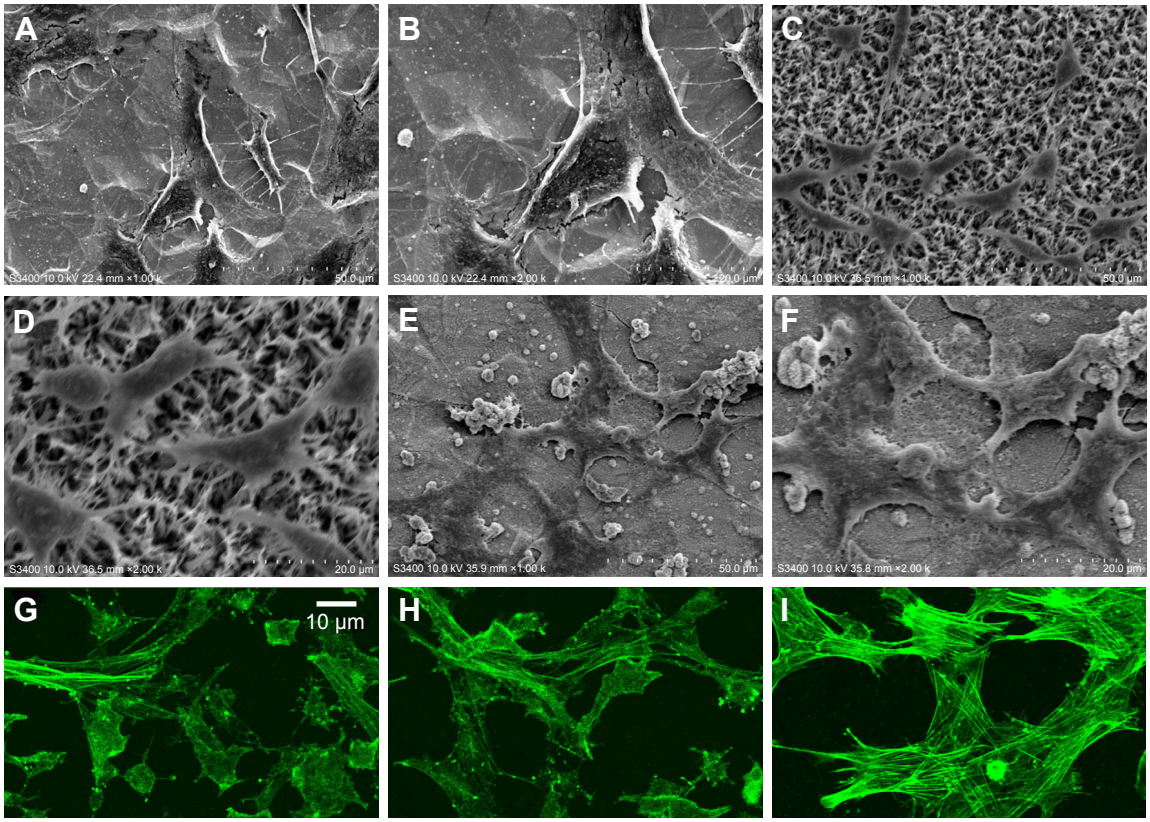

Figure 10 SEM morphologies of the MC3T3-E1 cells on bare Ti substrate (**A** and **B**), HA coating (**C** and **D**), and FAgHA coating (**E** and **F**); fluorescence microscopic images of MC3T3-E1 cells on the Ti (**G**), HA (**H**), and FAgHA (**I**) coatings after 24 hours of culture, actin were stained with phalloidin (green).
Abbreviations: SEM, scanning electron microscope; HA, hydroxyapatite; FAgHA, F-and-Ag-substituted HA.

of osteoblasts as shown by F-actin staining in Figure 10I. The cells exhibited contact guidance in the nanostructures of FAgHA/TNTs surface with nano-rod- and flake-like morphology; the osteoblasts became more extended with a fusiform-shaped morphology. Therefore, similar to the other two materials, the FAgHA/TNTs surface offers beneficial properties of osteoblast adhesion, which is in accordance with the MTT assay.

It has been found that 6 wt% Ag can notably inhibit the growth of cells, which leads to the death of a few osteoblasts.[58] However, we found that Ag did not affect the cell morphology, which could be because of a low doping amount of Ag (4.00 wt%). On the other hand, cell adhesion depends on the surface roughness.[59] Webster et al reported that nano-grained ceramics with surface structures <100 nm can improve the bioactivity of Ti implants and enhance osteoblast adhesion.[60,61] In this aspect, nanoscaled modification by FAgHA is an alternative route to improve the osseointegration of Ti-based orthopedic implants.[62,63] Kilpadi et al suggest that more cell proteins and more purified integrins can be attached to the HA than to commercial pure Ti or stainless steel.[64] In addition, cell adhesion protein absorption is more easily achieved on nano-sized materials because of their higher adhesion.[64,65]

Cell proliferation

The cytotoxicity of Ti, HA, and FAgHA/TNT coatings was determined by the MTT assay against the preosteoblast MC3T3 cells of mice (Figure 11A). The viability of the cells cultured on HA was comparable with that of the FAgHA/TNT sample. However, the Ag-doped FHA was a little toxic to MC3T3-E1, and the cell viability was slightly lower than that of the HA coating after 4 and 7 days ($p>0.5$); this can be due to the releasing of Ag^+, which results in a few negative effects or influencing the proliferation.[9,12] Interestingly, after culturing for 4 and 7 days, the cell viability of both the coatings increased obviously, and a statistical significance between the coatings and Ti was observed ($p<0.5$). Moreover, a lower release rate of silver ions can reduce their bioavailability and toxicity.[12] The results show that the behavior of the cultured cells is influenced by the F content; a low surface potential due to a high F content is favored by the cell attachment.[66] Meanwhile, the decrease of the FAgHA dissolution rate could inhibit the release of Ag^+,

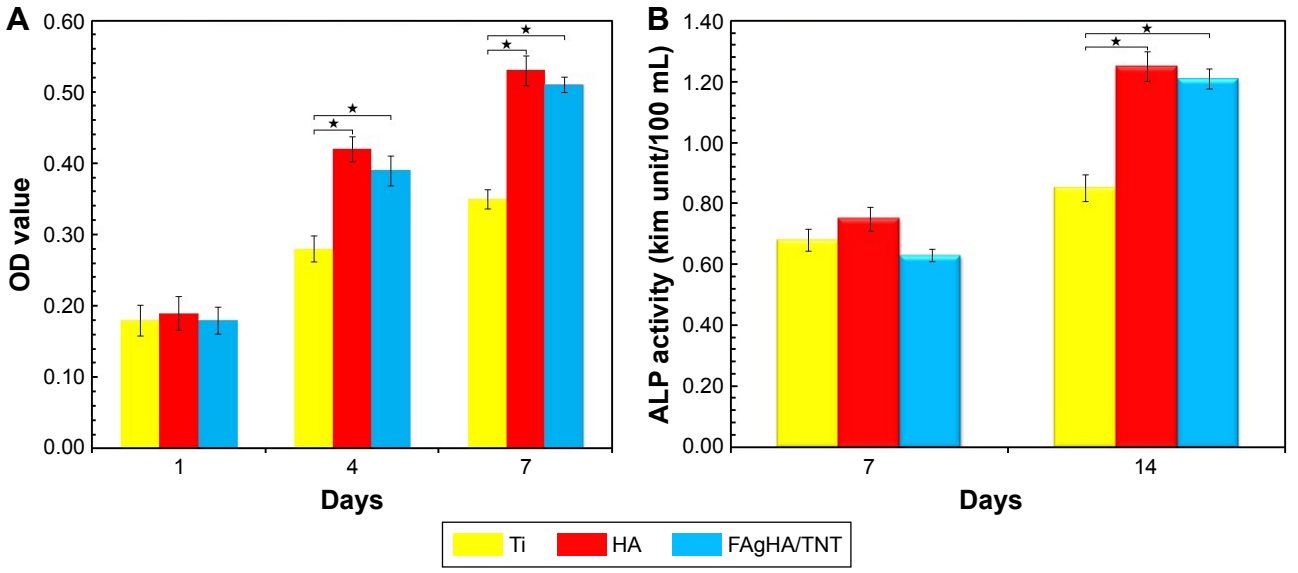

Figure 11 (**A**) MTT assay for the viability of osteoblasts cultured on bare Ti substrate, HA coating, and FAgHA coating at various incubation periods; (**B**) ALP activity of osteoblasts cultured on bare Ti substrate, HA coating, and FAgHA coating in 7 and 14 days. Data are presented as mean ± standard deviation (n=5), one-way ANOVA, (*$p<0.05$).

Abbreviations: MTT, 3-(4,5-dimethyl-2-thiazolyl)-2,5-diphenyl-2-H-tetrazolium bromide; HA, hydroxyapatite; ALP, alkaline phosphatase; TNT, titania nanotube; FAgHA, F-and-Ag-substituted HA.

thereby reducing its effect on cell proliferation.[23] Finally, the toxicity of Ag^+ is hindered, which contributed to the increase of cell viability in 7 days. Therefore, the biocompatibility of metallic implants could be controlled by modulating the bioavailability of the released Ag^+.

ALP activity test

The ALP activity is an indication of the early differentiation level of osteoblast cells, as it has an important role in promoting the formation of bone tissues at the surface of implants.[12] As illustrated in Figure 11B, the normalized ALP activity for all the samples increased after 7 and 14 days. When the cells were cultured on the FAgHA/TNT, on the 7th day, the ALP activity was lower than that for both Ti and HA, but not statistically ($p>0.5$). Interestingly, the FAgHA/TNT coating obviously increased the ALP activity of the cells than that of those cells cultured on the Ti surface on the 14th day ($p<0.5$); however, the ALP activity of the FAgHA/TNT coating was even lower than that of the HA, but not statistically ($p>0.5$); therefore, the FAgHA/TNT-coated sample promoted the differentiation of the MC3T3-E1 as compared with the bare Ti substrate. Chen et al demonstrated that co-sputtered Ag-HA coatings with a concentration of 2.05±0.55 wt% Ag show antimicrobial effects without cytotoxicity.[67] We have found that a 4.0 wt% Ag doping may influence the ALP secretion of osteoblast to a certain extent. Moreover, the aforementioned in vitro results suggest that the addition of F may reduce the toxicity of Ag nanoparticles in the coatings. In this study, Ag was incorporated into the HA coating to improve its antimicrobial properties. F was added as a second binary element to increase the structural stability and biocompatibility of the HA coating.

These results clearly confirm that the crystalline and morphological structure of nanocomposites improves the biocompatibility and dispersion ability in that the cells completely spread out and result in a nicely grown cell environment. The growth of the cells may be retarded by the roughness caused by the HA particles in microstructure composites, although nanocomposites themselves promote cell proliferation.[59] The FAgHA nanocomposite can be of great potential applications in the field of bone tissue engineering for the growth and cell proliferation of osteoblasts and bone formation. However, the possibility of toxicity due to the accumulation of Ag ions in body fluids raises the concern for the use of Ag in the FHA. Shi et al reported that the Ag-doping of 0.27 to 2.2 ppm leads to optimal properties with excellent cytocompatibility and antibacterial ability.[49] In our study, the highest Ag content for the FAgHA was 230 ppb which is considered low compared to other studies.[68,69] No significant difference was observed on cell proliferation and differentiation tests between HA and FAgHA, which implies no toxic effect of such amount of Ag ions. Their small amounts can even have positive effects on cells and can improve cytocompatibility.[59]

Apart from Ag^+, F^- ions can also influence the cell behavior through the FHA dissolution behavior. On the one hand, the existence of F in the FAgHA/TNT composites can make the cell attachment favorable through producing a low surface potential; on the other hand, the incorporated F can reduce the solubility of the FAgHA/TNT composites, which reduces the concentration of Ag^+ in the culture medium and, therefore, increases cell proliferation.[16] Therefore, the FAgHA composites with a moderate F content are thought to be promising, and they do demonstrate good performance both in vitro and in vivo. Overall, for clinical applications, a moderate content of F, such as $Ca_{10}(PO_4)_6(OH)_{0.52-1.33}F_{0.67-1.48}$, is reportedly most suitable as a compromise among cell adhesion, proliferation, and dissolution resistance.[38] Hence, we chose x=1.5 ($Ca_{10}(PO_4)_6(OH)_{2.0-x}F_x$) in the FAgHA/TNT composite.

In addition, it is worth considering that surface wettability also plays a significant role in osteoblast differentiation and osseointegration.[44] The results of this study indicate that a significant decrease of water CA was found in the HA-coated surfaces compared with the bare Ti substrate. This decreased water CA can stimulate cells to adhere and proliferate better.[44] Notably, the wettability results revealed that the mean CA of the control HA layer was even smaller than that of the FAgHA/TNT coating. However, the cell viability and ALP of the FAgHA/TNT were similar to those of the pure HA, which is an indication of good cytocompatibility. This finding means that the F release or the presence of Ag/F in the FAgHA/TNT coating was even more significant than wettability in promoting the cell growth and differentiation because the F release could induce cell proliferation and differentiation,[18] and the presence of F may alter the surface potential to enhance the cell attachment.[15]

Overall, interestingly enough, the incorporation of both Ag^+ and F^- ions into the HA allows for a combination of their individual functions for realizing an integrated set of their excellent properties such as 1) good mechanical performance, 2) long-term stability, 3) enhanced in vitro bioactivity, and 4) antibacterial behavior. These promising features of the FAgHA/TNT antibacterial bio-coating makes it very appealingly suitable for orthopedic applications. Essential for the preclinical evaluation, animal tests should be performed to examine the interaction of the FAgHA/TNT-coated implants with bone tissues.

Conclusion

F and Ag were uniformly simultaneously incorporated into the crystal structure of the HA without forming any other secondary phase. The nanostructured coatings of the FAgHA were successfully deposited onto Ti substrates through ED. The strength of the coatings was improved by a heat treatment that was carried out on the coated samples. Compared with the HA coating, the FAgHA/TNT coating was dense and uniform with a surface of nano-rods of diameters ranging from 30 to 50 nm. The solubility measurement indicated that the dissolution resistance of the HA was increased due to the incorporation of F^- ions. The corrosion resistance was enhanced by the nano-rod-like coating – the corrosion current density was decreased by nearly two orders of magnitude. The bonding strength was improved by >17 MPa, thanks to the anchoring effect of the TiO_2 nanotube layer. A superior bactericidal effect against viable *S. aureus* after the incubation with the FAgHA/TNT was found, whereas incubation with pure HA and control samples did not lead to any significant effects. The results of the immersion tests indicated that the FAgHA/TNT coating presented excellent biological activity. Through in vitro antibacterial and cell viability studies, it was found that the FAgHA/TNT bilayer coating on Ti exhibited excellent antibacterial properties and cytocompatibility. The results confirm that the nanostructured FAgHA/TNT coating is biocompatible and does not negatively impact MC3T3 proliferation and osteoblastic differentiation, whether or not Ag is present. The experimental HA coatings with the codoping of Ag and F ions were found to have integrated bactericidal and bioactive properties, which makes these coatings a promising surface treatment for orthopedic implants. These results pave the way for practical clinical applications of the FAgHA/TNT biocomposites as an antibacterial bio-coating.

Acknowledgments

This work was supported by the Second Batch of Young Talents Fund of Hebei Province, China; the Natural Science Foundation of Hebei Province, China (No H2016405008); National Natural Science Foundation of China (No 51377163, 11647159), China; the Youth Fund of Science and Technology of Hebei Colleges, China (No QN2017010); Population Health Information in Hebei Province Engineering Technology Research Center; and Science and Technology Research Project of Zhangjiakou, China (No 17120012D).

Disclosure

The authors report no conflicts of interest in this work.

References

1. Khalili V, Khalil-Allafi J, Frenzel J, Eggeler G. Bioactivity and electrochemical behavior of hydroxyapatite-silicon-multi walled carbon nano-tubes composite coatings synthesized by EPD on NiTi alloys in simulated body fluid. *Mater Sci Eng C*. 2017;71:473–482.

2. Đošic M, Erakovic S, Jankovic A, et al. In vitro investigation of electrophoretically deposited bioactive hydroxyapatite/chitosan coatings reinforced by graphene. *J Ind Eng Chem*. 2017;47:336–347.
3. Prodana M, Duta M, Ionita D, Bojina D, Stan MS, Dinischiotu A. Substituted hydroxyapatites for biomedical applications: a review. *Ceram Int*. 2015;41:6318–6325.
4. Mirzaee M, Vaezi M, Palizdar Y. Synthesis and characterization of silver doped hydroxyapatite nanocomposite coatings and evaluation of their antibacterial and corrosion resistance properties in simulated body fluid. *Mater Sci Eng C*. 2016;69:675–684.
5. Chozhanathmisra M, Ramya S, Kavitha L, Gopi D. Development of zinc-halloysite nanotube/minerals substituted hydroxyapatite bilayer coatings on titanium alloy for orthopedic applications. *Colloid Surface A*. 2016;511:357–365.
6. Subramani R, Elangomannan S, Louis K, Kannan S, Gopi D. Fabrication of minerals substituted porous hydroxyapaptite/poly(3,4-ethylenedioxy pyrrole-co-3,4-ethylenedioxythiophene) bilayer coatings on surgical grade stainless steel and its antibacterial and biological activities for orthopedic applications. *ACS Appl Mater Interfaces*. 2016;8:12404–12421.
7. Huang Y, Zhang HL, Qiao HX, et al. Anticorrosive effects and in vitro cytocompatibility of calcium silicate/zinc-doped hydroxyapatite composite coatings on titanium. *Appl Surf Sci*. 2015;357:1776–1784.
8. Huang Y, Xu ZW, Zhang XJ, et al. Nanotube-formed Ti substrates coated with silicate/silver co-doped hydroxyapatite as prospective materials for bone implants. *J Alloy Compd*. 2017;697:182–199.
9. Eraković S, Janković A, Ristoscu C, et al. Antifungal activity of Ag:hydroxyapatite thin films synthesized bypulsed laser deposition on Ti and Ti modified by TiO_2 nanotubes substrates. *Appl Surf Sci*. 2014;293:37–45.
10. Karamian E, Abdellahi M, Khandan A, Abdellah S. Introducing the fluorine doped natural hydroxyapatite-titania nanobiocomposite ceramic. *J Alloy Compd*. 2016;679:375–383.
11. Gao JY, Wang M, Shi C, Wang LP, Zhu YC, Wang DL. A facile green synthesis of trace Si, Sr and F multi-doped hydroxyapatite with enhanced biocompatibility and osteoconduction. *Mater Lett*. 2017;196:406–409.
12. Xu ZQ, Li M, Li X, et al. Antibacterial activity of silver doped titanate nanowires on Ti implants. *ACS Appl Mater Interfaces*. 2016;8:16584–16594.
13. López EO, Rossi AL, Archanjo BS, Ospina RO, Mello A, Rossi AM. Crystalline nano-coatings of fluorine-substituted hydroxyapatite produced by magnetron sputtering with high plasma confinement. *Surf Coat Tech*. 2015;264:163–174.
14. Wang J, Chao YL, Wan QB, Zhu ZM, Yu HY. Fluoridated hydroxyapatite coatings on titanium obtained by electrochemical deposition. *Acta Biomaterialia*. 2009;5:1798–1807.
15. Huang Y, Zhang XJ, Qiao HX, et al. Corrosion resistance and cytocompatibility studies of zinc-doped fluorohydroxyapatite nanocomposite coatings on titanium implant. *Ceram Int*. 2016;42:1903–1915.
16. Graziani G, Bianchi M, Sassoni E, Russo A, Marcacci M. Ion-substituted calcium phosphate coatings deposited by plasma-assisted techniques: a review. *Mater Sci Eng C Mater Biol Appl*. 2017;74:219–229.
17. Gokcekaya O, Webster TJ, Ueda K, Narushima T, Ergunc C. In vitro performance of Ag-incorporated hydroxyapatite and its adhesive porous coatings deposited by electrostatic spraying. *Mater Sci Eng C Mater Biol Appl*. 2017;77:556–564.
18. Huang Y, Qiao HX, Nian XF, et al. Improving the bioactivity and corrosion resistance properties of electrodeposited hydroxyapatite coating by dual doping of bivalent strontium and manganese ion. *Surf Coat Tech*. 2016;291:205–215.
19. Dey T, Roy P, Fabry B, Schmuki P. Anodic mesoporous TiO_2 layer on Ti for enhanced formation of biomimetic hydroxyapatite. *Acta Biomater*. 2011;7:1873–1879.
20. Suchanek K, Hajdyła M, Maximenko A, et al. The influence of nanoporous anodic titanium oxide substrates on the growth of the crystalline hydroxyapatite coatings. *Mater Chem Phys*. 2017;186:167–178.
21. Parcharoen Y, Kajitvichyanukul P, Sirivisoot S, Termsuksawad P. Hydroxyapatite electrodeposition on anodized titanium nanotubes for orthopedic applications. *Appl Surf Sci*. 2014;311:54–61.
22. Goudarzi M, Batmanghelich F, Afshar A, Dolati A, Mortazavi G. Development of electrophoretically deposited hydroxyapatite coatings on anodized nanotubular TiO_2 structures: corrosion and sintering temperature. *Appl Surf Sci*. 2014;301:250–257.
23. Zhao CL, Hou P, Ni JH, Han P, Chai YM, Zhang XN. Ag-incorporated FHA coating on pure Mg: degradation and in vitro antibacterial properties. *ACS Appl Mater Interfaces*. 2016;8:5093–5103.
24. Turkoz M, Atilla AO, Evis Z. Silver and fluoride doped hydroxyapatites: Investigation by microstructure, mechanical and antibacterial properties. *Ceram Int*. 2013;39:8925–8931.
25. Jegatheeswaran S, Selvam S, Sri Ramkumar V, Sundrarajan M. Facile green synthesis of silver doped fluor-hydroxyapatite/β-cyclodextrin nanocomposite in the dual acting fluorine-containing ionic liquid medium for bone substitute applications. *Appl Surf Sci*. 2016;371:468–478.
26. Yan YJ, Zhang XJ, Huang Y, Ding QQ, Pang XF. Antibacterial and bioactivity of silver substituted hydroxyapatite/TiO_2 nanotube composite coatings on titanium. *Appl Surf Sci*. 2014;314:348–357.
27. Huang Y, Yan YJ, Pang XF. Electrolytic deposition of fluorine-doped hydroxyapatite/ZrO_2 films on titanium for biomedical applications. *Ceram Int*. 2013;39:245–253.
28. Ahmadi S, Mohammadi I, Sadrnezhaad SK. Hydroxyapatite based and anodic titania nanotube biocomposite coatings: fabrication, characterization and electrochemical behavior. *Surf Coat Tech*. 2016;287:67–75.
29. Kokubo T, Takadama H. How useful is SBF in predicting in vivo bone bioactivity? *Biomaterials*. 2006;27:2907–2915.
30. Andrade FAC, Oliveira Vercik LC, Monteiro FJ, Silva Rigo EC. Preparation, characterization and antibacterial properties of silver nanoparticles–hydroxyapatite composites by a simple and eco-friendly method. *Ceram Int*. 2016;42:2271–2280.
31. Jeong YH, Choe HC, Brantley WA, Sohn IB. Hydroxyapatite thin film coatings on nanotube-formed Ti–35Nb–10Zr alloys after femtosecond laser texturing. *Surf Coat Technol*. 2013;217:13–22.
32. Geng Z, Cui ZD, Li ZY, et al. Strontium incorporation to optimize the antibacterial and biological characteristics of silver substituted hydroxyapatite coating. *Mater Sci Eng C Mater Biol Appl*. 2016;58:467–477.
33. Fahami A, Beall GW, Betancourt T. Synthesis, bioactivity and zeta potential investigations of chlorine and fluorine substituted hydroxyapatite. *Mater Sci Eng C Mater Biol Appl*. 2016;59:78–85.
34. Fowler BO. Infrared studies of apatites. I. Vibrational assignments for calcium, strontium, and barium hydroxyapatites utilizing isotopic substitution. *Inorg Chem*. 1974;13:194–207.
35. Boyd A, Randolph LD, Rutledge L, Meenan BJ. Strontium substituted hydroxyapatite coatings deposited via a co-deposition sputter technique. *Mater Sci Eng C Mater Biol Appl*. 2015;46:290–300.
36. Robinson L, Salma-Ancane K, Stipniece L, Meenan BJ, Boyd AR. The deposition of strontium and zinc Co-substituted hydroxyapatite coatings. *J Mater Sci Mater Med*. 2017;28:51–65.
37. Landis WJ, Martin JR. X-ray photoelectron spectroscopy applied to gold-decorated mineral standards of biological interest. *J Vac Sci Technol A*. 1984;2:1108–1111.
38. Bai Y, Bai YL, Gao JJ, Ma W, Su J, Jia RL. Preparation and characterization of reduced graphene oxide/fluorhydroxyapatite composites for medical implants. *J Alloy Compd*. 2016;688:657–667.
39. Branemark PI. Osseointegration and its experimental background. *J Prosthet Dent*. 1983;50:399–410.
40. Utku FS, Seckin E, Goller G, Tamerler C, Urgen M. Carbonated hydroxyapatite deposition at physiological temperature on ordered titanium oxide nanotubes using pulsed electrochemistry. *Ceram Int*. 2014;40:15479–15487.
41. Oh SH, Finones RR, Daraio C, Chen LH, Jin S. Growth of nano-scale hydroxyapatite using chemically treated titanium oxide nanotubes. *Biomaterials*. 2005;26:4938–4943.

42. Cheng K, Ren C, Weng W, et al. Bonding strength of fluoridated hydroxyapatite coatings: a comparative study on pull-out and scratch analysis. *Thin Solid Films*. 2009;517:5361–5364.
43. Yang YC, Chang E. Influence of residual stress on bonding strength and fracture of plasma-sprayed hydroxyapatite coatings on Ti–6Al–4V substrate. *Biomaterials*. 2001;22:1827–1836.
44. Huang JY, Zhang XC, Yan WX, et al. Nanotubular topography enhances the bioactivity of titanium implants. *Nanomedicine*. 2017;13:1913–1923.
45. Wang YQ, Tao J, Wang L, He PT, Wang T. HA coating on titanium with nanotubular anodized TiO_2 intermediate layer via electrochemical deposition. *Trans Nonferrous Metals Soc China*. 2008;18:631–635.
46. Dubnika A, Loca D, Rudovica V, Parekh MB, Berzina-Cimdina L. Functionalized silver doped hydroxyapatite scaffolds for controlled simultaneous silver ion and drug delivery. *Ceram Int*. 2017;43:3698–3705.
47. Hardes J, Ahrens H, Gebert C, et al. Lack of toxicological sideeffects in silver-coated megaprostheses in humans. *Biomaterials*. 2007;28:2869–2875.
48. Kang S, Herzberg M, Rodrigues DF, Elimelech M. Antibacterial effects of carbon nanotubes: size does matter. *Langmuir*. 2008;24:6409–6413.
49. Shi C, Gao JY, Wang M, Fu JK, Wang DL, Zhu YC. Ultra-trace silver-doped hydroxyapatite with non-cytotoxicity and effective antibacterial activity. *Mater Sci Eng C Mater Biol Appl*. 2015;55:497–505.
50. Xiu ZM, Zhang QB, Puppala HL, Colvin VL, Alvarez PJJ. Negligible particle-specific antibacterial activity of silver nanoparticles. *Nano Lett*. 2012;12:4271–4275.
51. Jung WK, Koo HC, Kim KW, Shin S, Kim SH, Park YH. Antibacterial activity and mechanism of action of the silver ion in Staphylococcus aureus and Escherichia coli. *Appl Environ Microbiol*. 2008;74:2171–2178.
52. Feng QL, Wu J, Chen GQ, Cui FZ, Kim TN, Kim JO. A mechanistic study of the antibacterial effect of silver ions on Escherichia coli and Staphylococcus aureus. *J Biomed Mater Res*. 2000;52:662–668.
53. Gosheger G, Hardes J, Ahrens H, et al. Silver-coated megaendoprostheses in a rabbitmodel – an analysis of the infection rate and toxicological side effects. *Biomaterials*. 2004;25:5547–5556.
54. Noda I, Miyaji F, Ando Y, et al. Next generation antibacterial hydroxyapatite coating: antibacterial activity of Ag ions in serum. *Bioceram Dev Appl*. 2010;1:1–3.
55. Oktar F. Characterization of processed tooth hydroxyapatite for potential biomedical implant applications. *Artif Cells Blood Substit Biotechnol*. 1999;27:367–379.
56. Janković A, Eraković S, Mitrić M, et al. Bioactive hydroxyapatite/grapheme composite coating and its corrosion stability in simulated body fluid. *J Alloys Compd*. 2015;624:148–157.
57. Zhang L, Liu W, Yue C, et al. A tough grapheme nanosheet/hydroxyapatite composite with improved in vitro biocompatibility. *Carbon*. 2013;61:105–115.
58. Fielding GA, Roy M, Bandyopadhyay A, Bose S. Antibacterial and biological characteristics of silver containing and strontium doped plasma sprayed hydroxyapatite coatings. *Acta Biomater*. 2012;8:3144–3152.
59. Bostancioglu RB, Gurbuz M, Akyurekli AG, Dogan A, Koparal AS, Koparal AT. Adhesion profile and differentiation capacity of human adipose tissue derived mesenchymal stem cells grown on metal ion (Zn, Ag and Cu) doped hydroxyapatite nano-coated surfaces. *Colloid Surface B*. 2017;155:415–428.
60. Webster TJ, Ergun C, Doremus RH, Siegel RW, Bizios R. Specific proteins mediate enhanced osteoblast adhesion on nanophase ceramics. *J Biomed Mater Res*. 2000;51:475–483.
61. Webster TJ, Schadler LS, Siegel RW, Bizios R. Mechanisms of enhanced osteoblast adhesion on nanophase alumina involve vitronectin. *Tissue Eng*. 2001;7:291–301.
62. Chung TW, Liu DZ, Wang SY, Wang SS. Enhancement of the growth of human endothelial cells by surface roughness at nanometer scale. *Biomaterials*. 2003;24:4655–4661.
63. Webster TJ, Ejiofor JU. Increased osteoblast adhesion on nanophase metals: Ti, Ti6Al4V, and CoCrMo. *Biomaterials*. 2004;25:4731–4739.
64. Kilpadi KL, Chang P-L, Bellis SL. Hydroxylapatite binds more serum proteins, purified integrins, and osteoblast precursor cells than titanium or steel. *J Biomed Mater Res*. 2001;57:258–267.
65. Liu H, Webster TJ. Nanomedicine for implants: a review of studies and necessary experimental tools. *Biomaterials*. 2007;28:354–369.
66. Li JN, Song Y, Zhang SX, et al. In vitro responses of human bone marrow stromal cells to a fluoridated hydroxyapatite coated biodegradable MgeZn alloy. *Biomaterials*. 2010;31:5782–5788.
67. Chen W, Liu Y, Courtney HS, et al. In vitro antibacterial and biological properties of magnetron co-sputtered silver-containing hydroxyapatite coating. *Biomaterials*. 2006;27:5512–5517.
68. Rameshbabu N, Kumar TSS, Prabhakar TG, Sastry VS, Murty KVGK, Rao KP. Antibacterial nanosized silver substituted hydroxyapatite: synthesis and characterization. *J Biomed Mater Res A*. 2007;80:581–591.
69. Gokcekaya O, Ueda K, Narushima T, Ergun C. Synthesis and characterization of Ag containing calcium phosphates with various Ca/P ratios. *Mater Sci Eng C*. 2015;53:111–119.